Qiu *et al. Virology Journal* (2025) 22:166
https://doi.org/10.1186/s12985-025-02796-6

Virology Journal

RESEARCH Open Access

Integrated in-silico design and in vivo validation of multi-epitope vaccines for norovirus

Jingxuan Qiu[1†], Yiwen Wei[1†], Jiayi Shu[2†], Wenjing Zheng[3], Yuxi Zhang[1], Junting Xie[1], Dong Zhang[1], Xiaochuan Luo[1], Xiulan Sun[4], Xin Wang[1,5], Sijie Wang[3*], Xuanyi Wang[3*] and Tianyi Qiu[2*]

Abstract

Background Norovirus (NoVs) is a foodborne pathogen that causes acute gastroenteritis. The diversity of its principal antigenic protein poses a significant challenge to vaccine development and the prevention of large-scale outbreaks globally. Currently, no licensed vaccines against norovirus have been approved.

Methods We developed a novel pipeline that integrates multiple bioinformatics tools to design broad-spectrum vaccines against NoVs. Specifically, broad-spectrum T-cell epitope vaccines were designed based on consensus sequences and optimized epitope screening, while broad-spectrum B-cell spatial epitope vaccines were constructed using high-throughput antigenicity calculations and epitope mapping.

Results This pipeline underwent rigorous validation at three levels: firstly, In silico validation: Analysis of properties and structures demonstrated the appropriateness of amino acid composition and the structural integrity of the vaccine sequences. Secondly, theoretical assessment: Evaluation of human leukocyte antigen (HLA) subtype and antigenicity coverage indicated a broad theoretical protective spectrum for the designed vaccine immunogens. Furthermore, in silico simulation confirmed their ability to elicit an immune response. Finally, animal-level validation: Experiments in mice showed that both vaccine immunogens stimulated high levels of IgG and IgA. Notably, Vac-B induced a strong IgG response against GII.2 and a robust IgA response against GII.17, comparable to the immune response elicited by the wild-type NoV non-replicating virus-like particle (VLP) protein group.

Conclusions Both in silico and in vivo experimental findings suggest that the proposed pipeline and vaccine immunogens could serve as valuable theoretical guidance for the development of multi-epitope vaccines against NoVs.

†Jingxuan Qiu, Yiwen Wei and Jiayi Shu contributed equally to this work.

*Correspondence:
Sijie Wang
sijieW@outlook.com
Xuanyi Wang
xywang@shmu.edu.cn
Tianyi Qiu
qiu.tianyi@zs-hospital.sh.cn

Full list of author information is available at the end of the article

Keywords Norovirus, Multi-epitopes vaccine, Broad-spectrum, B-cell spatial epitope, T-cell epitope

Introduction

Norovirus is the primary non-bacterial cause of acute gastroenteritis outbreaks and sporadic cases globally, spreading via contaminated food, water, direct or indirect contact, and aerosols [1, 2]. While most infections subside within 24 h without treatment [3], they pose life-threatening risks to young children, the elderly, and immunocompromised individuals [1]. Annually, norovirus causes approximately 700 million infections, 219,000 deaths, and billions in economic impact worldwide [4], highlighting the urgent need for effective prevention strategies.

Norovirus is a positive-sense single-stranded RNA virus belonging to the *Caliciviridae* family [5]. Noroviruses are classified into 12 genogroups (GI–GX, GNA1, and GNA2) based on their structural proteins, although only viruses from GI, GII, GIV, GVIII, and GIX genogroups are capable of infecting humans [6]. Multiple genotypes have been associated with large-scale gastroenteritis [7]. The major structural protein VP1 and the minor structural protein VP2 are key antigenic components, with VP1 being widely utilized in the development of various vaccines [8].

Vaccination is an effective means of prevention. However, no licensed vaccines are currently available to prevent norovirus infection. The genetic diversity of circulating norovirus strains, limited understanding of immune response to natural infection, and the absence of established immune correlates of protection represent key challenges in developing an effective norovirus vaccine [9]. Three types of vaccine candidates have been developed and are currently undergoing clinical trials: VLPs, P particles, and recombinant adenovirus-based vaccines [9]. These candidates are capable of providing protection against disease caused by specific target genotypes. However, it remains uncertain whether they can elicit cross-immune responses to heterologous norovirus strains, i.e., strains not included in the vaccine formulation. Serological studies of the Takeda vaccine in Phase IIb clinical trials have shown that vaccine efficacy may vary depending on the exposure history of the target population [10]. Similarly, the Vaxart oral vaccine has not demonstrated a consistent immune response to heterologous strains in clinical settings [11]. Therefore, the development of a multivalent vaccine is urgently required to provide broad protection against a diverse range of circulating norovirus strains.

Several technological breakthroughs have significantly advanced vaccine design. The advent of massively parallel DNA sequencing, high-throughput discovery of protective human antibodies, sequencing of the B cell repertoire, and increasing structural characterization of protective antigens and epitopes have provided more detailed and comprehensive insights into vaccine development. Bioinformatics approaches to protein antigen selection, collectively referred to as Reverse Vaccinology (RV), have largely supplanted classical vaccinology, which is labour-intensive and time-consuming due to its dependence on pathogen cultivation [12]. In addition, in-silico methods were successfully applied in the development of drugs. For example, the utilization of microarray datasets and bioinformatics analysis illustrated the prospects of structure-based drug design [13]; multi-stage computational-biophysics correlate could identify the potential drug molecules [14]; Nadeem's work developed a novel therapeutic approaches that integrating networking biology, molecular docking and simulation tools [15]; latest work of Nimra's has developed an optimized deep learning approach to determine the exact brain permeability value for a possible drug [16]. The successful application of computational methods in drug development has demonstrated the high efficiency of bioinformatics in target discovery and protein design. In recent years, multi-epitope vaccines have been regarded as an ideal strategy for the prevention of tumors and virus infections [17]. Numerous researchers have investigated and designed multi-epitope subunit vaccines targeting various viruses, including the influenza virus [18], Coxsackievirus B3 [19], Crimean-Congo hemorrhagic fever virus [20], Monkeypox virus [21], among others. For the construction of multi-epitope vaccine, in silico design including epitope prediction, vaccine construction, computational evaluation of broad coverage has been developed and applied on different pathogens antigens including spike protein for SARS-CoV-2 [22], EG95 for E. granulosus [23], and SRS protein for Toxoplasma gondii [24]. These researches illustrated the application of computational vaccine design and provided promising candidate vaccines for preclinical studies.

An ideal multi-epitope vaccine should incorporate multiple epitopes, allowing each structural unit—each antigenic peptide segment—to stimulate cytotoxic T lymphocytes, helper T cells, and B cells, thereby generating effective immune responses against a specific tumor or virus [17]. The judicious selection of B cell epitopes and T cell epitopes is a critical aspect of vaccine design, as these epitopes greatly influence the efficacy of epitope-based vaccines by eliciting both humoral and cellular immune responses [25].

Thus, the prediction and screening of epitopes using computational methods are indispensable steps in silico design of multi-epitope vaccines. Numerous in silico

prediction tools are available for identifying B cell epitopes, including general antigenic region-based methods such as DiscoTope [26] and SEPPA [27], as well as antibody-based methods like EpiPred [28]. T cell epitopes prediction tools include motif-based approaches such as PREDIVAC [29] and Propred-I [30], alongside machine learning-based platforms like NetMHC [31] and EpiTOP [32]. Despite the availability of a wide array of epitope prediction resources, there is currently no suitable and comprehensive pipeline that integrates the diverse tools required at each stage for norovirus multi-epitope vaccine development.

Given the complexity of B cell epitope identification [33], previous studies on norovirus multi-epitope vaccines have predominantly focused on selection of T cell epitopes and B cell linear epitopes, while conformational epitopes have generally been excluded from vaccine design [8, 34]. Owing to the genotypic and antigenic diversity of norovirus, current research has emphasized immune stimulation targeting the major circulating strains, with cross-immune responses to other, less-studied yet clinically relevant strains not considered a central focus of vaccine development [35]. However, the development of broad-spectrum epitopes is essential, as such epitopes could activate immune responses against the majority of known strains and potentially confer protection against future variants. In this study, we established an integrated pipeline for designing broad-spectrum multi-epitope vaccines against norovirus. The pipeline was developed through analysis of all known human norovirus genotypes, incorporating the full range of collected VP1 and VP2 proteins.

Unlike previously developed vaccines that are based on individual proteins or proteomes from one or a few genotypes, our approach involves the prediction of linear epitopes for both T cells and B cells, while also incorporating conformational immune epitopes using bioinformatics tools-an aspect frequently overlooked in prior research. The final vaccine construct designed using this method is capable of inducing immune responses and providing cross-protection against diverse norovirus genotypes.

In contrast to other studies on norovirus multi-epitope vaccines, our work offers detailed insights into these key components. Importantly, the immunogenicity and broad-spectrum efficacy of the vaccines produced via this pipeline has been validated in in vitro experiments. Thus, both the designed vaccine and the proposed pipeline present substantial advantages for future norovirus vaccine development.

Method

Dataset

For vaccine construction, four categories of data were required: (1) amino acid sequences of VP1 and VP2 protein from different norovirus genotypes, (2) three-dimensional structure of VP1 protein, (3) sequence and structure of previously reported vaccine protein, and (4) B cell spatial epitopes.

(1) Reference nucleotide sequences of capsid protein for norovirus were collected from the Human Calicivirus Typing Tool (2022.12.08) (the access link can be seen in Table S1). All partial or full nucleotide sequences of VP1 and VP2 were fetched and aligned with ClustalX 2.1 [36]. Then nucleotide sequences of VP1 and VP2 were translated into protein sequences using EMBOSS-transeq tool [37] (the access link can be seen in Table S1). In total, 212 VP1 and 146 VP2 protein sequences were retained in the dataset, covering five genogroups-GI, GII, GIV, GVIII, and GIX, corresponding to 43 genotypes including 10 from GI, 29 from GII, 2 from GIV, and 1 each from GVIII and GIX, respectively (Table S2).

(2) The three-dimensional structures of VP1 proteins were constructed using Modeller 10.4 [38], with homology modeling templates selected from existing PDB entries in the most up-to-date database (specifically, protein models with PDB IDs: 1IHM, 6OTF, 7K6V, and 6OU9). Structures with fewer than 500 amino acids were excluded. Structural quality was assessed using SAVES v6.0, and poorly modelled structures were refined via the Robetta server [39]. Due to a lack of suitable structural templates, VP2 structures were not constructed. Ultimately, a total of 190 VP1 protein structures were included in the dataset.

(3) To enable comparison of vaccine performance, the experimentally validated vaccine protein GII.4C(GII.4 Consensus VLPs), reported in the literature, was selected as a positive control [40]. GII.4C is a consensus sequence derived from three genetically distinct, naturally occurring GII.4 strains. The sequence was collected, and the structure was modelled using Modeller 10.4.

(4) Known B cell spatial epitope positions were obtained from published literature [41–46]. The spatial coordination of epitopes were extracted from corresponding VP1-antibody complex PDB structures. The final dataset comprised 26 available epitopes, and 4 from GI.1, 1 from GII.3, 6 from GII.10, 11 from GII.4, and 4 from GII.17 (Table S3).

The multi-epitope vaccine construct

B cell multi-epitope vaccine construction

Mapping of B cell Spatial epitopes

To compare reported B cell spatial epitopes, the positions of various epitope residues were mapped onto each of the 190 VP1 structures included in the constructed Dataset 2. Firstly, the residue positions of 26 epitopes from Dataset 4 were compiled. Subsequently, the corresponding residue positions in each VP1 structure were determined via multiple sequence alignments, performed in accordance

with the method described in Sect. *T cell Multi-Epitope Vaccine Construct*. Finally, the spatial locations of each epitope were annotated on every VP1 structure, including the representative GII.4C structure.

Selection of broad-spectrum epitopes

A key strategy for vaccines to achieve broad-spectrum immunity involves the utilization of one or more antigens with broad reactivity to elicit immune protection against predominant viral strains. Accordingly, evaluating cross-reactivity (i.e., antigenic similarity) is of crucial importance. In this study, CE-BLAST [51] was employed to quantify the antigenic similarity of each epitope.

The spatial coordinates of epitopes within each VP1 structure were input into CE-BLAST, which then computed pairwise antigenic similarity scores. An epitope with a similarity score exceeding 0.7 was considered to possess high antigenic similarity. The antigenic coverage of each epitope within each VP1 structure was calculated as the proportion of structurally similar proteins. Epitopes with antigenic coverage greater than 50% were classified as broad-spectrum B-cell epitopes. Among these, those with coverage exceeding 75% were designated as major epitopes, while the remainder were classified as minor epitopes. For a complete protein comprising multiple epitopes, the overall antigenic coverage was defined as the union set of epitope coverages.

Construct B cell multi-epitope vaccine

Among the 190 VP1 structures in Dataset 2, those containing the greatest number of major epitopes were selected as vaccine templates. Minor epitopes were subsequently assembled onto the selected template, resulting in final B-cell multi-epitope vaccine construct, Vac-B. The three-dimensional structure of Vac-B was modelled using Modeller 10.4.

T cell multi-epitope vaccine construct

The multiple sequence alignments for VP1 and VP2 in Dataset 1 were performed using ClustalX 2.1. The consensus sequences were generated by selecting the most frequently occurring amino acids at each position. The consensus sequence of the VP1 protein (VP1-con) comprised 519 amino acids, while that of VP2 (VP2-con) consisted of 227 amino acids. Major Histocompatibility Complex (MHC) class I and II binding peptides within VP1-con and VP2-con were subsequently predicted using tools provided by the Immune Epitope Database (IEDB).

For MHC class I binding prediction, the reference HLA set consisted of 27 allele, offering over 97% global population coverage [47]. Peptide lengths were set to 9–10 amino acids. The IEDB T Cell Epitope Prediction tool, using the recommended NetMHCpan4.1 EL algorithm [48], was employed. The tool outputs a percentile rank score representing binding affinity to specific MHC molecules; lower scores indicate a higher probability of epitope presentation. Peptides ranking within top 1% were selected for further analysis.

For MHC class II binding prediction, the reference HLA panel included 27 commonly occurring DR, DQ, and DP alleles, collectively covering more than 99% population [49]. Peptide lengths was set between 12 and18 amino acids, statistically encompassing approximately 82.89% of known epitope lengths. The IEDB MHC-II Binding Prediction tool, using the recommended IEDB 2.22 method [50], was applied. As with class I, lower percentile rank scores denote stronger predicted binding. Peptides within the top 10% were selected, aligning with IEDB's recommended threshold (top 1% for MHC-I and top 10% for MHC-II).

Based on these predicted peptides, potential broad-spectrum epitopes were identified through the following steps:

Step1. Definition of candidate sites (CS)

Each residue within the sequence of a selected MHC class I and or II binding peptide was designated as a candidate site (CS).

Step2. The screen of broad-spectrum sites CS-B

For all CS within MHC class I peptides derived from VP1 and VP2, CS-Bs were defined as sites capable of binding to more than 10 or 5 different HLA subtypes, respectively. For MHC class II peptides, CS-Bs were those capable of binding to more than 8 or 4 HLA subtypes, respectively.

Step3. Construction of broad-spectrum epitopes (E-B)

Within VP1 and VP2, adjacent CS-Bs were conjoined to construct broad-spectrum epitopes (E-Bs). E-Bs shorter than 8 amino acids for MHC-I or 9 amino acids for MHC-II were excluded. Final E-B sequences were extended by three amino acids at both the N- and C-termini to enhance binding potential. Vaccine constructs were assembled by linking the selected E-Bs using AAY and GPGPG linkers. Three vaccine constructs were generated, Vac-VP1, Vac-VP2, and Vac-VP1-VP2 (Table S4). In addition, broad-spectrum epitopes from the positive control vaccine sequence were also identified following the same process, enabling a comparative analysis of broad-spectrum efficacy among constructs.

Prediction of constructed vaccine protein

Allergenicity, antigenicity, toxicity, and solubility

The allergenicity of the vaccine constructs was using AlgPred v.2.0 [52] and AllergenFP v1.1 servers [53]. The VaxiJen v2.0 [54] server was used to determine the probable antigenicity of the designed vaccine constructs using

an alignment-independent algorithm with a threshold of 0.4. The toxicity of the proposed vaccines was analyzed using the ToxinPred2 server [55]. And the propensity of vaccine constructs to be soluble on overexpression in *E.coli* were assessed by SOLpro [56].

Physicochemical characterization

The ProtParam, a tool from the Expasy server [57] was used to characterize protein physicochemical properties, including molecular weight, aliphatic index, isoelectric pH, hydropathicity, GRAVY values, instability index, and estimated half-life.

Transmembrane topology and secondary structure analysis

DeepTMHMM [58] was used to predict transmembrane helices in the proteins. The PSIPRED v4.0 tool [59] was employed to predict the alpha helices, beta sheets, and coils of the vaccine proteins.

Validation of vaccine constructs

Three-dimensional modeling of the potential vaccine candidates, and structure refinement

The 3D structures of the three T-cell vaccine constructs were predicted using the Robetta web server. The GalaxyWEB server [60] was employed to refine the predicted 3D structures. The refined structures were evaluated using tools. Such as the Ramachandran plot and G-factors (via the PROCHECK server) [61]. ERRAT [62] analysis and Z-score analysis (via the ProSA-web server) [63] were also performed for the vaccine constructs.

Molecular Docking between vaccine constructs and toll-like receptors, HLA allele-epitopes interaction

Molecular Docking between vaccine constructs and toll-like receptors

Effective recognition between antigens and Toll-like receptors (TLRs) is essential for generating an appropriate immune response. The potential binding interactions between the vaccine constructs and TLRs were predicted. Human TLR-7, which plays a key role in initiating immune responses against viral infections, was selected as the receptor. The three-dimensional structure of human TLR-7 (PDBID: 7CYN) was retrieved from the Protein Data Bank [64].

Molecular docking between the structurally verified vaccine structures and TLRs was carried out using the ClusPro 2.0 server [65], and the resulting interaction patterns were visualized using the PDBsum web server [66].

Molecular Docking simulation of the HLA allele-epitopes interaction

The AlphaFold3.0 server [67] was employed to model the conformational structure of designed broad-spectrum T-cell peptides. The molecule docking between different HLA molecules and T-cell peptides was performed by ClusPro 2.0 [65]. The 3D structure of HLA subtypes in the corresponding reference sets were collected from PDB database. Among them, the MHC I alleles with population frequency over 10% [68–70] and all five MHC II alleles which have experimentally structures were selected for the further molecular docking with T-cell epitopes (Table S5).

Immune simulation

The immune response elicited by the designed vaccine constructs was stimulated using the C-ImmSim server [71], which evaluated parameters such as antibody titer, T cell population, and B cell population. In C-IMMSIM, each simulated time step corresponds to eight hours in real life. The simulation protocol for the three vaccine constructs followed that of the positive control (GII.4C) reported in a previous study, involving two injections administered 21 days apart, with a total of 1050 simulation steps [40].

Molecular dynamic simulation

After structure refinement of four vaccine constructs, the molecular dynamics simulation (MD) was conducted for Vac-VP1, Vac-VP2, Vac-VP1-VP2, Vac-B and positive control GII.4C protein, the structure deformability and flexibility were evaluated by iMODS [72–74] and CABS-flex [75].

Codon adaptation and in Silico cloning of the vaccine construct

The codon adaptation tool (JCat) was introduced to adapt the codon usage to the host for accelerating the expression rate in it [8]. *Escherichia coli* is the most popular prokaryote host, meanwhile, mammalian cells and yeast are the most used eukaryotic host [76]. Thus, all three types were chosen as the targeted hosts. SnapGene (www.snapgene.com) were used to insert the optimized sequence into pET30a(+) vector between the BamHI [77] and XhoI [78].

In vitro expression, purification and experiments of constructed vaccines

Protein expression and purification

The full-length genes of Vac-B and Vac-VP1-VP2 were synthesised by Sangon Biotech (Shanghai, China). The synthesised genes were sub-cloned into a modified pET-30a vector using *NdeI/XhoI* restriction sites, and the plasmids were subsequently transformed into *Escherichia coli* strain BL21(DE3). Transformants were cultured at 37 °C until reaching an OD600 of 0.6, and protein expression was induced with 0.4 mM IPTG. Following 20 h of incubation at 16 °C, cells expressing Vac-B and Vac-VP1-VP2

proteins were lysed. The resulting supernatant was purified using Ni-NTA affinity chromatography, followed by ion exchange and gel filtration chromatography. Purified proteins were analysed using Sodium Dodecyl Sulfate-Polyacrylamide Gel Electrophoresis (SDS-PAGE) and visualised with Coomassie blue staining.

Purified protein samples were quantified using the bicinchoninic acid (BCA) assay (Beyotime Biotechnology), following the manufacturer's instructions. Equal amounts of protein were mixed with SDS-PAGE loading buffer, heated at 99 °C for 5 min, and separated on a 4–12% Bis-Tris gradient precast gel (MeiunBio) via SDS-PAGE. Proteins were then transferred to a polyvinylidene difluoride (PVDF) membrane (Immobilon®-P, Sigma) using the Trans-Blot Turbo rapid wet transfer system (Genscript), according to the manufacturer's protocol. Membranes were blocked for 15 min at room temperature using a commercial rapid blocking solution (QuickBlock™ Blocking Buffer, Beyotime Biotechnology), and then incubated overnight at 4 °C with immunized mouse serum (1:5000 dilution) as the primary antibody, prepared in commercial antibody diluent (QuickBlock™ Primary Antibody Dilution Buffer, Beyotime Biotechnology). After three washes with TBS-T (20 mM Tris-HCl, 150 mM NaCl, 0.1% Tween-20), membranes were incubated for 1 h at room temperature with HRP-conjugated goat anti-mouse IgG (1:5000), diluted in the same antibody diluent. Protein bands were visualized using enhanced chemiluminescence (ECL; Tanon), and images were acquired using a fully automated chemiluminescence imaging system (Tanon). Band intensities were quantified using ImageJ software.

Mice and ethics statement

The 4-week-old specific-pathogen-free (SPF) female BALB/c mice were purchased from Charles River Laboratories (Massachusetts, United States), and housed under SPF conditions. All animal experiments were conducted in accordance with the standards set by the Ethics Committee of Fudan University. Forty 4-week-old female SPF (Specific Pathogen Free) BALB/c mice were randomly divided into four groups ($n = 10$ per group): the Vac-VP1-VP2 immunization group, the Vac-B immunization group, the positive control group, and the negative control group. Mice in the positive control group were immunized with a hexavalent norovirus vaccine candidate (under development, not yet marketed) produced by Anhui Zhifei Longcom Biopharmaceutical Co., Ltd., while mice in the negative control group were injected with adjuvant-containing saline. Each mouse received three immunisations at 14-day intervals. The administered antigen solution consisted of 0.8 mg/ml of protein mixed in equal volume with adjuvant.

The anesthesia protocol for mice was as follows: an intraperitoneal injection of 0.3% sodium pentobarbital solution at a dose of 50 mg/kg. Blood samples were collected via the submandibular venous plexus Euthanasia was performed by cervical dislocation following anesthesia. The animal studies in this paper are approved by the Ethics Committee of the Institutes of Biomedical Sciences, Fudan University, with the approval number of No.174.

Vac-B- and Vac-VP1-VP2-specific IgG and IgA level in the serum measured by ELISA

Sera were collected 14 days after the final immunization and stored at -80 °C. ELISA plates were coated with 100 µL of 0.5 µg/ml monovalent protein stock solution of ReNoV GI.1, GII.2, GII.3, GII.4, GII.6, and GII.17 virus-like praticles (VLPs), and incubated overnight at 4 °C. The plates were then washed three times and blocked with 5% bovine serum albumin (BSA), followed by incubation with appropriately diluted sera. Horseradish peroxidase (HRP)-conjugated goat anti-mouse IgG or IgA was subsequently added, followed by tetramethylbenzidine (TMB) substrate. The enzymatic reaction was stopped, and absorbance was measured at OD450/620nm using a microplate reader.

Statistical analysis

Signal-to-noise ratio (S/N) was calculated based on the OD450/620 values of the test serum (specimen, S) and the negative control (N). A test serum was considered positive when $S/N \geq 2.1$. The IgG/IgA antibodies in the test serum was expressed as the reciprocal of the highest dilution yielding a positive result. The detection system employed serum from non-immunised mice as the negative reference. Serum sample with IgG/IgA antibody titers ≥ 40 is classified as positive [79].

$$\mathrm{GMT} = lg^{-1}\left(\frac{\sum f.lg\,X}{\sum f}\right)$$

Data were analysed using Stata (v17.0) and GraphPad Prism (v9.0) software. The 95% confidence interval (95% CI) was calculated using the Clopper-Pearson method. Both the P-value and 95% CI were evaluated using two-sided tests, with $P < 0.05$ considered statistically significant.

For the analysis of specific IgG and IgA antibody titers, the geometric mean titer (GMT) and 95% CI were used to describe the average antibody titer levels. The GMT was calculated by taking the inverse logarithm of the mean of the log-transformed original antibody titers. Pearson's chi-square test was used to assess intergroup differences between groups. Graphs were generated using GraphPad Prism (v9.0) software, with statistical

significance annotated as follows: ns, $P > 0.05$; *, $P < 0.05$; **, $P < 0.01$; ***, $P < 0.001$; ****, $P < 0.0001$.

Results

Construction of vaccines

In this study, we developed a pipeline for the construction of broad-spectrum vaccines targeting norovirus. We first compiled a comprehensive dataset comprising 358 sequences, 190 three-dimensional structures, and 26 B-cell epitope annotations of the principal antigenic protein-the capsid protein of norovirus (Table S2 & Table S3, Fig. S1a). Subsequently, vaccine immunogens were generated using a multi-epitope vaccine construction strategy encompassing both T-cell and B-cell epitopes. Specifically, T-cell vaccine epitopes were selected based on peptide-MHC binding ability derived from consensus sequences of the capsid protein (see *Methods*), while B-cell vaccine epitopes were designed based on spatial epitopes that demonstrated both antigenicity and broad-spectrum protective potential (see *Methods*). Finally, we conducted a comprehensive evaluation of the generated vaccine constructs in comparison with the experimentally validated vaccine sequence GII.4C, employing both in-silico and in-vivo experiments. The overall workflow of this study is illustrated in Fig. 1.

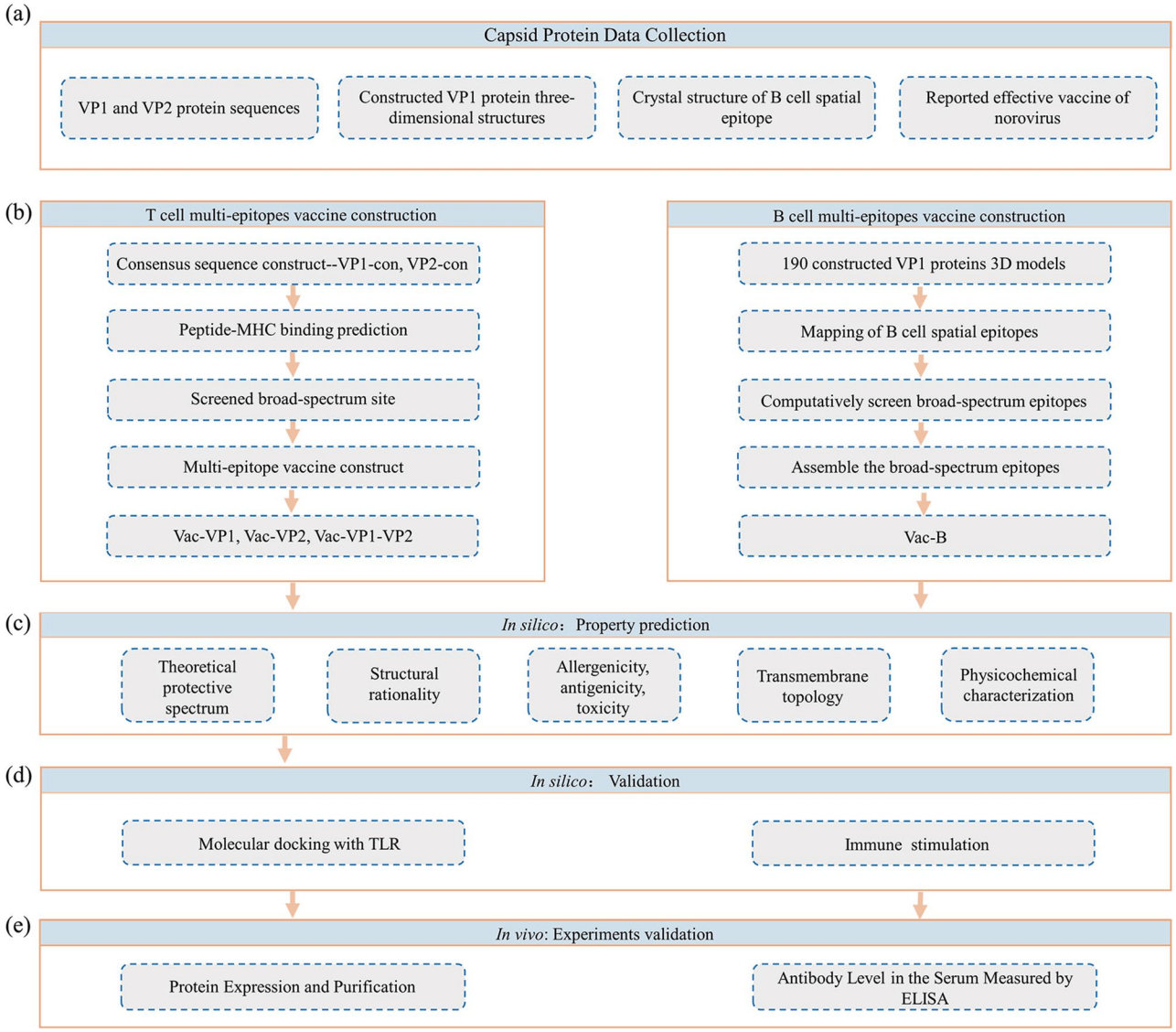

Fig. 1 Workflow of vaccine design in this study. (**a**) Construction of datasets; (**b**) Design of multi-epitope vaccines, comprising two distinct strategies for T-cell and B-cell vaccines, respectively; (**c**) In silico characterisation of the constructed vaccine proteins, including prediction of theoretical protective spectrum, structural validity, allergenicity, antigenicity, toxicity, physicochemical properties, and transmembrane topology; (**d**) In silico validation of the designed vaccines, encompassing molecular docking with Toll-like receptors and immune simulation; (**e**) Experimental validation of the designed vaccines, including in vitro expression and purification of antigens, and in vivo murine immunisation experiments

High theoretical protective spectrum of designed multi-epitope vaccine candidates

The theoretical protective spectrum of designed T-cell multi-epitope vaccine candidates

Based on the proposed strategy for broad-spectrum epitope selection (see *Methods T cell Multi-Epitope Vaccine Construct*), we identified 9 E-B for MHC-I and 7 E-B for MHC-II binding within VP1-con. Epitope coverage was defined as the union of all covered positions; accordingly, these epitopes exhibited strong binding affinity with over 55% and 30% of HLA subtypes in the respective reference sets.

For VP2-con, we identified 5 E-B for MHC-I and 3 for MHC-II, which demonstrated high binding affinity with over 55% and 25% of HLA subtypes, respectively. For GII.4C, 13 E-B epitopes for MHC-I and 7 for MHC-II were identified, showing high binding affinity with over 45% and 40% of HLA subtypes. The extent of broad-spectrum HLA coverage conferred by our vaccine constructs is comparable to that of the reported norovirus vaccine candidate GII.4C. Epitope lengths and their associated HLA subtype coverage are presented in Fig. 2b. The constructed VP1-con and VP2-con sequences in this study demonstrated broad theoretical protective potential and could provide protection-wide immunological coverage.

The multi-epitope vaccine was constructed by linking the selected MHC-I and MHC-II epitopes using peptide linkers. AAY linkers were attached to the MHC-I binding epitopes, which may facilitate formation of suitable sites for binding to the transporter associated with antigen processing transporters (TAP), thereby enhancing epitope presentation [80]. GPGPG linkers were used to join MHC-II binding epitopes, as they help prevent junctional immunogenicity, preserve the immunogenicity of individual epitopes, and stimulate T-helper lymphocyte responses [81].

The final lengths of the designed vaccine constructs Vac-VP1, Vac-VP2, and Vac-VP1-VP2 were 425, 206, and 634 amino acids, respectively. The schematic representation of the topology of the final vaccine candidate is shown in Fig. 2a.

The assemble of broad-spectrum epitopes and construction of Vac-B vaccine candidate

To design a B-cell multi-epitope vaccine, 26 spatial B-cell spatial epitopes were collected from published literature. Within the VP1 protein, the P domain forms the outward-facing protrusion and contains the determinants of cell attachment as well as principal antigenic sites [82]. As illustrated in Fig. S1a, the locations of these 26 collected

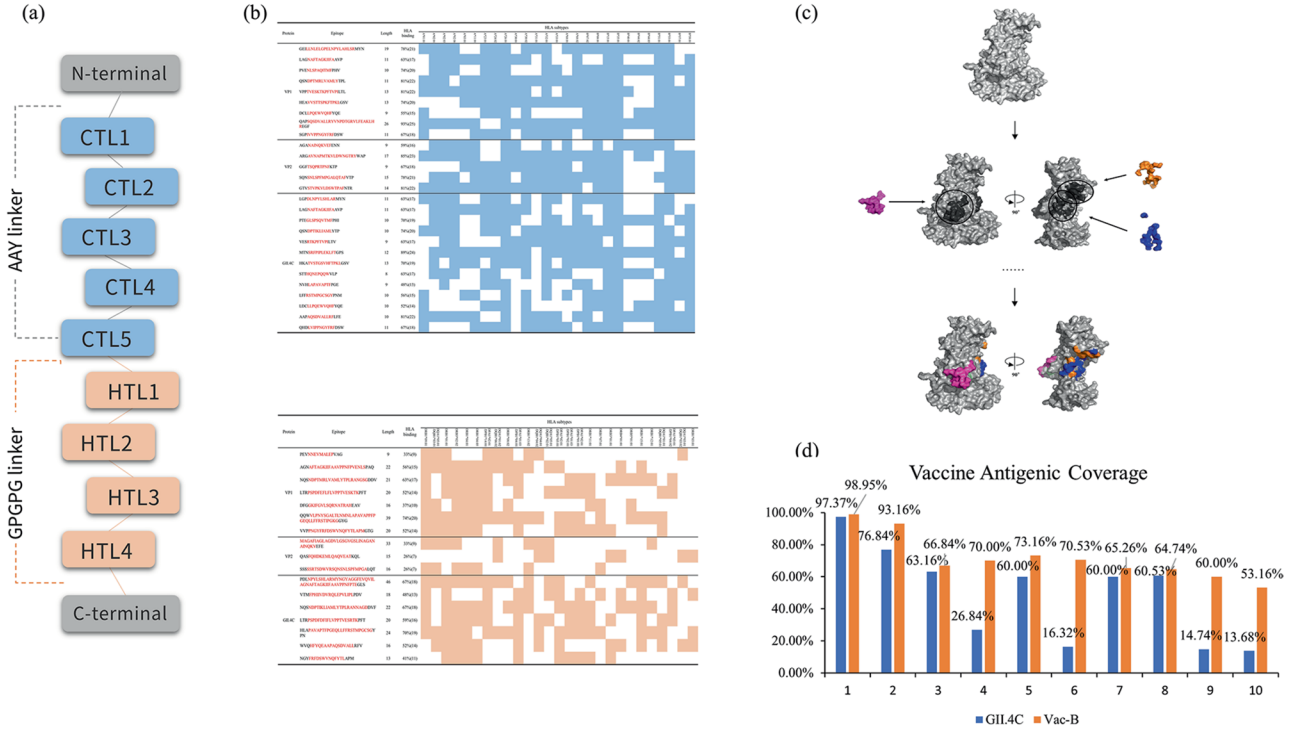

Fig. 2 Results of the constructed vaccine candidates and their theoretical protective spectra. (**a**) Schematic illustration of the multi-epitope vaccine: blue boxes represent MHC-I epitopes, while orange boxes represent MHC-II epitopes. (**b**) Length and HLA protective coverage of the designed epitopes: the upper panel displays MHC-I epitopes, and the lower panel displays MHC-II epitopes. (**c**) Stepwise assembly of broad-spectrum epitopes and vaccine design: first, the three-dimensional model structure of the selected template is shown; second, minor epitope positions are mapped and incorporated into the template; finally, the assembled three-dimensional model structure is presented. (**d**) Antigenic coverage of Vac-B and GII.4 C for each epitope. PyMOL 2.6.0a0 [84] was used to visualize spatial localization

epitopes span the majority of the exposed surface of the P domain, enabling a comprehensive evaluation of immune recognition.

Among these 26 reported epitopes, 10 achieved antigenic coverage of over 50% across all VP1 antigens and were therefore defined as broad-spectrum epitopes (Table S6, Figs. S1b and S1c). These formed the foundation for assembly. Of these, five epitopes conferred antigenic coverage of ≥ 75% across all VP1 antigens and were classified as major epitopes (Table S6, Fig. S1c), while the remaining broad-spectrum epitopes were designated as minor epitopes. The detailed CE-BLAST similarity scores for all 26 epitopes could be seen in Supplementary File 2.

Template protein selection for epitope assembly was based on epitope coverage. The ideal template satisfied the following criteria:

1. The provided complete (100%) joint coverage of the five major epitopes. Among the 190 proteins analyzed, AY675554, AB190457, KJ196278, and KX907728 fulfilled this requirement.
2. It exhibited substantial overlap in individual cross-reactive coverage of the five major epitopes.

Based on these criteria, AY675554 was selected as the template protein for epitope assembly. For the positions of minor epitope, the most representative epitopes-those offering highest antigenic coverage- were assembled by substituting the amino acids at the corresponding positions.

The three-dimensional structure of the resulting vaccine candidate, Vac-B, was modelled using Modeller 10.4. The assembly progress is depicted in Fig. 2c, and the full amino acid sequence of Vac-B is provided in Table S4, the discontinuous B cell epitopes on the three-dimensional structure of Vac-B were shown in Fig. S2 and Table S7.

The evaluation of Vac-B involved calculating its theoretical coverage:

a) Individual coverage of each of the 10 epitopes:

To assess antigenicity, the reported vaccine candidate GII.4C was also evaluated. As shown in Fig. 2d, the individual epitope coverage in GII.4C was uneven, with the lowest coverage-epitope 10 (from PDB 8EN5)-achieving only 13.68%. In contrast, for the designed Vac-B in this model, each epitope exhibited broad antigenic coverage exceeding 50%, with an average coverage of 71.58%.

b) Joint coverage of the 10 epitopes:

The overall antigenic coverage of Vac-B was 100%, surpassing the 99.47% achieved by GII.4C. Among all VP1 proteins, JQ613567 was not covered by GII.4C. The particular protein belongs to the human norovirus GIV.1 strain, which was responsible for two small-scale outbreaks of acute gastroenteritis among elderly individuals in Australia [83].

In conclusion, the assembled Vac-B in this study may provide broad cross-protection across multiple norovirus genotypes, demonstrating strong potential as a broad-spectrum vaccine candidate.

Structural rationality of designed T-cell multi-epitope vaccine candidates

The secondary and tertiary structures of proteins can offer valuable insights into ligand-binding sites and potential molecular functions, serving as a foundation for subsequent investigations [85, 86]. The predicted secondary structure of the vaccine constructs, obtained via PSIPRED, revealed that Vac-VP1 comprised 7.29% α-helix, 22.35% β-strand, and 70.35% random coil. Vac-VP2 exhibited 36.41% α-helix, 6.31% β-strand, and 57.28% random coil. The Vac-VP1-VP2 construct consisted of 20.03% α-helix, 20.66% β-strand, and 59.31% random coil. For Vac-B, the secondary structure included 6.52% α-helix, 27.93% β-strand, and 65.55% random coil. These detailed results are presented in Table 1.

It has been reported that the flexible spatial configuration of random coils facilitates epitope formation [87], suggesting that the abundance of random coils in vaccine constructs may favor immune recognition.

For each vaccine construct, five structural models were generated (Table S8). To enhance the accuracy of the predicted structures, the model with the highest scores based on Ramachandran plot and ERRAT evaluations was selected. Model 4 for Vac-VP1, model 5 for Vac-VP1-VP2, and model 3 for Vac-B were selected for further refinement via the GalaxyWEB platform, while model 4 for Vac-VP2 was retained without further modification.

An ideal structural model is characterized by a high proportion of residues located within the most favored region of the Ramachandran plot, with minimal residues in outlier regions [86]. A model with over 90% of residues in the most favored regions is typically considered of excellent quality [88]. Following refinement, the percentage of residues in favored regions improved as follows: Vac-VP1 (87.9%), Vac-VP2 (90.7%), Vac-VP1-VP2 (84.4%), and Vac-B (92.7%). The proportions of residues in disallowed regions were reduced to 1.9%, 0.6%, 0.8%, and 0.0%, respectively (Table 1), indicating high-quality structural models.

To further verify the structural integrity of the final vaccine constructs, ProSA-web and ERRAT were employed. Structural plausibility was assessed using Z-scores from ProSA-web, which compare the construct to known protein structures in the PDB database. Z-scores falling outside the native range suggest potential structural errors

Table 1 The properties and validation results of the vaccine constructs

Vaccine Constructs		Vac-VP1		Vac-VP2		Vac-VP1-VP2		Vac-B	
Antigenicity (Threshold 0.4)		0.4635		0.4665		0.4640		0.4909	
Allergenicity		Non-Allergen		Allergen/Non-Allergen		Non-Allergen		Non-Allergen	
Toxicity		Non-Toxin		Non-Toxin		Non-Toxin		Non-Toxin	
Topology		Outer Membrane		Outer Membrane		Outer Membrane		Outer Membrane	
Molecular weight		45032.29 Da		21325.72 Da		66645.32 Da		58453.11	
Theoretical pI		5.72		8.97		6.22		5.55	
Aliphatic index		75.79		59.37		70.41		82.96	
GRAVY		-0.059		-0.307		-0.136		-0.188	
Instability Index score		36.82 (stable)		32.08(stable)		35.67(stable)		39.50(stable)	
Half-life		30 h (mammalian reticulocytes, in-vitro)		4.4 h (mammalian reticulocytes, in-vitro)		30 h (mammalian reticulocytes, in-vitro)		30 h (mammalian reticulocytes, in-vitro)	
		> 20 h (yeast, in-vivo)		> 20 h (yeast, in-vivo)		> 20 h (yeast, in-vivo)		> 20 h (yeast, in-vivo)	
		> 10 h (E. coli, in-vivo)		> 10 h (E. coli, in-vivo)		> 10 h (E. coli, in-vivo)		> 10 h (E. coli, in-vivo)	
Secondary Structure Analysis		7.294% helix		36.41% helix		20.03% helix		6.518% helix	
		22.35% strand		6.311% strand		20.66% strand		27.93% strand	
		70.35% coil		57.28% coil		59.91% coil		65.55% coil	
Refined model		before	after	before	after	before	after	before	after
ERRAT		73.82	73.52	97.35	-	85.07	83.74	51.83	94.64
Z-score		-5.71	-5.71	-4.02	-	-5.22	-5.32	-6.63	-6.81
Ramachandran Plot	Most favored	80.4%	87.9%	90.7%	-	77.7%	84.4%	89.7%	92.7
	Additional allowed	16.5%	10.2%	8.6%	-	20.5%	13.3%	9.6%	6.4
	Generously allowed	1.2%	0.0%	0.0%	-	1.0%	1.4%	0.5%	0.9
	Disallowed	1.9%	1.9%	0.6%	-	0.85%	0.8%	0.2%	0.0

[89]. Post-refinement, the Z-scores for Vac-VP1 (– 5.71), Vac-VP2 (– 4.02), and Vac-B (– 6.81) were all within the expected range for experimentally determined proteins of similar size. The Z-score for Vac-VP1-VP2 was – 5.32, slightly outside the typical range; however, its ERRAT overall quality factor was 83.74—well above the 50-point threshold, which indicates good structural quality [78, 90]. The ERRAT scores for Vac-VP1, Vac-VP2, and Vac-B were 73.52, 97.35, and 94.64, respectively (Figs. 3e, S3e–S5e). These two evaluation indices confirm that the refined three-dimensional structures of the vaccine candidates are of high quality and suitable for downstream analyses. Structural indices for Vac-VP1-VP2 are shown in Fig. 3, while structural validation of the remaining constructs can be found in Supplementary Figs. S3–S5.

Rational physic-chemical properties, solubility, high antigenicity, non-allergenicity, and non-toxicity of designed multi-epitope vaccine candidates

Ideal vaccines should elicit robust immune responses while avoiding allergenic or toxic effects [91]. Meanwhile, the physicochemical properties of vaccines—such as hydrophobicity, pH, and instability index—are critical for assessing their stability and biological activity [8, 92]. The subcellular localization of vaccines is also important, as proteins situated on the pathogen surface or within the secretome are the first to interact with the host and represent promising vaccine candidates [93]. Furthermore, the presence of transmembrane helices complicates the study and cloning of vaccine proteins [93]. Numerous computational tools are available to validate these properties. Accordingly, the antigenicity, allergenicity, toxicity, topography, and physicochemical characteristics—including molecular weight, instability index, aliphatic index, grand average of hydropathicity (GRAVY), and half-life—of the constructed vaccines were assessed using in silico methods.

Antigenicity of designed multi-epitope vaccine candidates

Antigenicity scores, which reflect the potential of the designed proteins to act as protective immunogens, were calculated using VaxiJen (v2.0). Higher scores indicate a greater likelihood of inducing protective immunity [94]. The default threshold for VaxiJen is 0.4. The results revealed antigenicity scores of 0.4635 for Vac-VP1, 0.4665 for Vac-VP2, 0.4640 for Vac-VP1-VP2, and 0.4909 for Vac-B, suggesting that all four proteins possess the potential to function as protective antigens.

Initially, we generated an epitope pool which including 252,658 previously validated peptides from IEDB(2025.05.08) [95]. By substring searching through

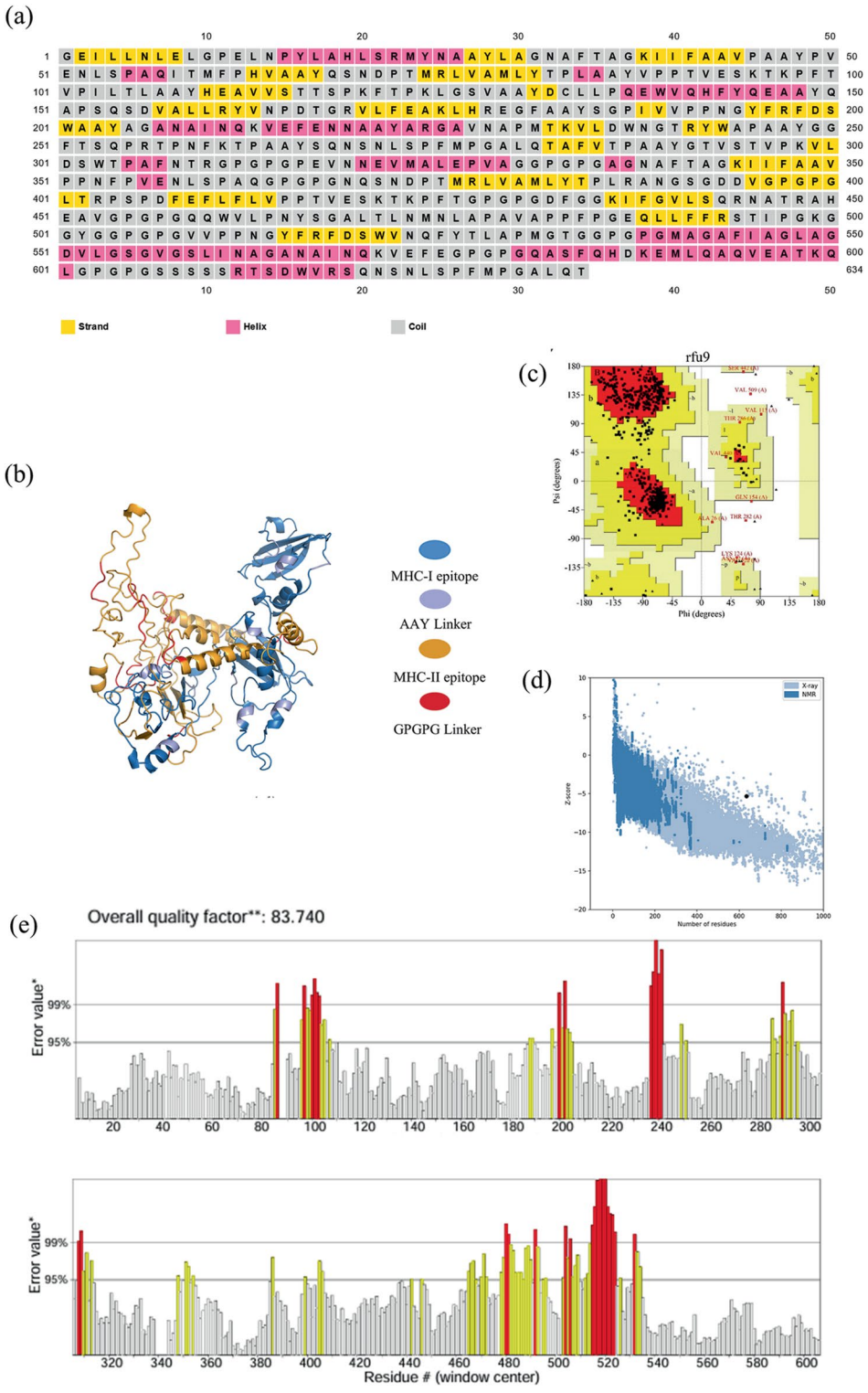

Fig. 3 Structural analysis and validation of the Vac-VP1-VP2 vaccine construct. (**a**) Predicted secondary structure of the multi-epitope vaccine, with β-strands shown in yellow, α-helices in pink, and random coils in grey. (**b**) Refined three-dimensional structure of the constructed vaccine shown in cartoon representation. (**c**) Ramachandran plot of the refined vaccine structure, indicating stereochemical quality. (**d**) Z-score of −5.32 for the refined protein model. The Z-score plot displays the typical score range for all protein chains of similar size in the PDB database, as determined by X-ray crystallography (light blue) and NMR spectroscopy (dark blue). The black dot represents the Z-score of the input protein. (**e**) ERRAT overall quality factor; a score above 50 is generally considered indicative of good structural quality

the epitope pool, 7 epitopes designed in this study were detected as previously validated peptides (Table S9), which illustrated the good performance of TSBSline to screening positive peptides.

In addition, we introducing IFNepitope [96] to predict the IFN-γ inducing potential of MHC binder peptides. Results showed that ten epitopes including five involved in VP1-con ("GEILLNLELGPELNPYLAHLSRMYN", "QSNDPTMRLVAMLYTPL", "VPPTVESKTKPFTVPILTL", "LTRPSPDFEFLFLVPPTVESKTKPFT" and "VVPPNGYFRFDSWVNQFYTLAPMGTG") and five involved in VP2-con ("ARGAVNAPMTKVLDWNGTRYWAP", "SQNSNLSPFMPGALQTAFVTP", "GTVSTVPKVLDSWTPAFNTR", "QASFQHDKEMLQAQVEATKQL" and "SSSSSRTSDWVRSQNSNLSPFMPGALQT") were predicted that hold the capability of IFN-γ production.

Finally, besides the concentration of antibodies, counts of helper T cells and cytotoxic T cells, the C-IMMSIM server [71] also simulates the concentration of cytokines and interleukins. Based on the results, all four vaccine candidates could induce the large titer scales of IFN-γ > 400,000 ng/ml, equivalent as the positive control GII.4C protein. All four vaccine candidates also exhibited the ability of inducing other cytokines, such as IL-4, IL-12, TGF-b.

Allergenicity, toxicity, solubility

In addition to antigenicity, we also assessed the allergenicity and toxicity of the designed proteins. All four constructs passed the allergenicity assessment, evaluated using AllergenFP (v1.1), and were confirmed to be non-toxic based on predictions by ToxinPred2. Furthermore, all four proteins were predicted to be outer membrane proteins by DeepTMHMM. Detailed characteristics of the proteins are presented in Table 1. We also evaluated the solubility upon overexpression of vaccines by SOLpro, all four constructs showed solubility above threshold value 0.5 [56] (0.5556, 0.9345, 0.6700, 0.7123 for Vac-VP1, Vac-VP2, Vac-VP1-VP2, and Vac-B). The predicted SOLpro results indicated that the designed vaccines are water-soluble on overexpression which is a prerequisite for many structural, functional and biochemical studies.

Rational physic-chemical properties

We also evaluated the physicochemical properties of the four designed proteins. The molecular weights were 45.03 kDa for Vac-VP1, 21.33 kDa for Vac-VP2, 66.65 kDa for Vac-VP1-VP2, and 58.45 kDa for Vac-B. These values, all below 110 kDa, suggest that the vaccine constructs are amenable to purification and are suitable for vaccine applications [97]. The computed instability indices were 36.82 (Vac-VP1), 32.08 (Vac-VP2), 35.67 (Vac-VP1-VP2), and 39.50 (Vac-B), all below the threshold of 40, indicating good protein stability.

The aliphatic indices were 75.79, 59.37, 70.41, and 82.96 for Vac-VP1, Vac-VP2, Vac-VP1-VP2, and Vac-B, respectively. These values fall within the distribution observed in thermostable proteins (mean 78.8, standard deviation 14.5), suggesting that the constructs possess favorable thermostability [98]. The GRAVY index (grand average of hydropathicity), which measures the mean hydropathy value across all amino acids in a protein, indicates whether a protein is hydrophilic or hydrophobic. Positive values denote hydrophobicity, whereas negative values indicate hydrophilicity, with lower values reflecting better solubility [99]. The GRAVY scores for the constructs were −0.059 (Vac-VP1), −0.307 (Vac-VP2), −0.136 (Vac-VP1-VP2), and −0.188 (Vac-B), indicating a favorable level of polarity and water solubility [100]. The estimated in vitro half-lives of Vac-VP1, Vac-VP1-VP2, and Vac-B in mammalian reticulocytes were 30 h. Their estimated in vivo half-lives were over 20 h in yeast and over 10 h in *E. coli*. For Vac-VP2, the in vitro half-life was 4.4 h in mammalian reticulocytes, with in vivo half-lives exceeding 20 h in yeast and 10 h in *E. coli*. These predictions are based on the N-end rule, which estimates protein half-life ranging from under 2 min to over 100 h. A 30-hour half-life in mammalian systems suggests sufficient duration for robust immune activation [101]. The predicted in vivo half-life of Vac-VP2 also indicates adequate persistence to ensure immunological efficacy. Taken together, these physicochemical properties confirm the suitability of all four constructs for vaccine development.

The validation result of T-cell potential vaccine candidates

Molecular Docking with innate receptors

Molecular Docking simulation of the TLR-peptide interaction

Toll-like receptors (TLRs) are innate immune receptors in mammals that function as sensors, capable of initiating and coordinating both innate and subsequent adaptive immune responses [102, 103]. Successful docking with sufficiently high affinity may serve as an indicator that a vaccine has the potential to elicit an immune response under physiological conditions [76]. Given that TLR7 recognises single-stranded RNA (ssRNA) and is capable of inducing innate immune responses to ssRNA viruses [104], along with its moderate to high expression levels in various intestinal epithelial cells—key targets during norovirus infection [104], docking analyses were performed using ClusPro 2.0. The extracellular or ectodomains (ECDs) of TLR7 were treated as the receptor, and the vaccine constructs as ligands, as ECDs are primarily responsible for ligand binding [102]. The experimentally validated vaccine GII.4C, as reported in the literature, was used as a positive control. ClusPro 2.0 generated

30 vaccine–receptor complexes (clusters) for each construct. Among these, the following selection criteria were applied:

(1) the docking complex with the lowest binding energy was selected;
(2) the docking pose had to avoid steric hindrance—specifically, the vaccine needed to dock on the distal portion of the TLR facing the cell membrane.

For Vac-VP1, clusters 4 and 17 were selected, with docking scores of – 1306.4 and – 1122.9, respectively. Within these complexes, multiple salt bridges, hydrogen bonds, and non-bonded contacts were predicted, including salt bridges such as ASP–LYS, ASP–HIS, ARG–ASP, and ARG–GLU (Table 2), and hydrogen bonds at the interaction interface (Table S10). The spatial configuration of the binding complex is shown in Fig. S6. Docking results for the remaining vaccine constructs are summarized in Tables S10–S17 and Figs. S7–S9. For the positive control GII.4C, clusters 18 and 11 were selected, with docking scores of – 1279.3 and – 1150.6, respectively. These values are comparable to those of the designed vaccine constructs, indicating that their predicted binding affinities are similar to the positive control (Fig. S10, Tables S18–S19). The predicted interactions between the vaccine constructs and TLR7 suggest plausible binding modes and support the potential of these vaccines to be recognized by innate immune receptors.

Molecular Docking simulation of the HLA allele-peptide interaction

Further, the binding affinity between MHC molecules and potential T-cell epitopes were predicted by ClusPro2.0 [65]. To set a benchmark, the most frequent HLA-I allele of HLA-A*02:01 and HLA-II allele of HLA-DRB1*01:01 were selected as examples. The original complexes between above allele and corresponding peptides were retrieved from PDB [64] as positive controls. It can be found that the predicted scores were ranged from – 1134.2 to -755.5 for HLA-I benchmark and were ranged from – 926.6 to -770.7 for HLA-II benchmark, respectively.

Meanwhile, the docking score between T-cell peptides proposed in this study and most frequent HLA alleles were calculated by ClusPro 2.0. As been illustrated in Fig. 4a, for HLA-I, 72.45% of the docking scores follows in the range of the benchmark, with 27.55% out of

Table 2 Docking scores of the vaccines and positive control with TLR7 receptor

Vaccine construct	Cluster	Docking score	Interacting residues
Vac-VP1	4	-1306.4	4 Salt bridges: ASP410(a)-LYS32(b); ASP285(a)-HIS86(b); ARG75(a)-ASP89(b); ARG408(a)-GLU802(b) 16 Hydrogen bonds 232 non-bonded contacts
	17	-1122.9	1 Salt bridges: ARG335(a)-ASP244(b) 17 Hydrogen bonds 279 non-bonded contacts
Vac-VP2	18	-1235.7	14 Hydrogen bonds 204 non-bonded contacts
	15	-1064.4	19 Hydrogen bonds 297 non-bonded contacts
Vac-VP1-VP2	2	-1331	13 Hydrogen bonds 189 non-bonded contacts
	28	-1054.9	5 Salt bridges: GLU111(a)-LYS108(b); GLU138(a)-LYS108(b); ASP301(a)-LYS197(b); GLU419(a)-LYS197(b); ASP587(a)-LYS274(b) 25 Hydrogen bonds 286 non-bonded contacts
Vac-B	4	-1195.8	7 Salt bridges: GLU61(a)-LYS32(b); ASP515(a)-LYS32(b); ARG92(a)-ASP89(b); ASP478(a)-LYS776(b); GLU485(a)-HIS800(b); ARG481(a)-GLU802(b); ARG535(a)-GLU802(b) 30 Hydrogen bonds 361 non-bonded contacts
	12	-1092.6	6 Salt bridges: LYS4(a)-ASP320(b); LYS4(a)-ASP346(b); GLU102(a)-LYS432(b); ASP11(a)-ARG473(b); GLU23(a)-LYS502(b); GLU150(a)-LYS502(b) 16 Hydrogen bonds 320 non-bonded contacts
GII.4 C	18	-1279.3	4 Salt bridges: ASP7(a)-LYS114(b); ASP7(a)-ARG115(b); ASP506(a)-LYS502(b); ARG345(a)-CLU583(b) 23 Hydrogen bonds 251 non-bonded contacts
	11	-1150.6	1 Salt bridges: GLU25(a)-LYS502(b) 13 Hydrogen bonds 167 non-bonded contacts

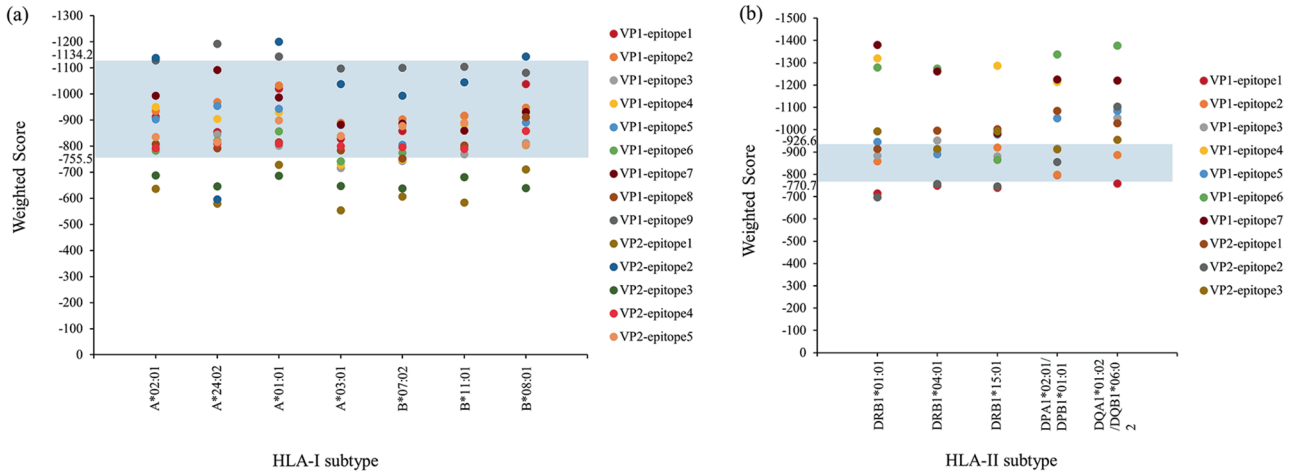

Fig. 4 Predicted weighted scores of peptides-HLA alleles. (**a**) Binding scores between selected HLA-I alleles and peptides, (**b**) Binding scores between selected HLA-II alleles and peptides

the range. Similarly, for HLA-II, 86.00% of the docking scores follows in the range with 14.00% out of the range (Fig. 4b). The docking results illustrated that most of the designed epitopes hold the potential to form stable peptide-HLA complexes. The detailed binding scores between all peptide-HLA complexes involved in this study can be found in Supplementary File 3.

The immune simulation result

The immune simulation result of T-cell vaccine constructs

To investigate the potency of the vaccine constructs in triggering immune responses, an in-silico simulation of the vaccine response was conducted using C-ImmSim. The concentration of antibodies, along with counts of helper T cells and cytotoxic T cells, were tested.

1. **Antibody concentration**: After the first injection of all vaccine antigens, antibodies began to be generated, and Vac-VP2 showed the highest level of antibody titres (over 20,000 of Vac-VP2, with the others showing titres of less than 20,000 per ml). All the antibody titres peaked after the second dose, and all the vaccine constructs induced large titre scales of > 80,000 per ml, which were superior to the validated vaccine GII.4C (positive control), which induced titres of < 80,000 per ml. Among these, Vac-VP1-VP2 exhibited the highest level of antibodies with close to 100,000 titre per ml. After 30 days of vaccine injection, antibody titres started to reduce rapidly and remained at a low level. At 100 days, the antibody titre of Vac-VP1-VP2 was higher than that of GII.4C (Fig. 5a).
2. **Immune Cell Count**: The number of T-helper cells showed a similar trend. Small peaks in total T-helper cells were observed after the first administration of all vaccines, with Vac-VP2 showing the highest level, while the others were roughly similar to GII.4C. The number of total T-helper cells reached its highest peak after the second administration. The T-helper cell peaks of the three vaccine constructs exceeded 10,000 cells per mm^3, which was higher than GII.4C. The number of T-helper memory cells gradually declined after the second dose. After 350 days, the T-helper cells of the vaccine constructs exceeded 500 cells per mm^3, which was higher than GII.4C (Fig. 5b). The simulation revealed that Vac-VP1 induced cytotoxic T-cells, with a peak of over 1,150 cells per mm^3 after the first administration, showing a stronger response compared to GII.4 C. For Vac-VP2 and Vac-VP1-VP2, the response was slightly lower, but an effective amount of cytotoxic T cells was still triggered (Fig. 5c).
3. **Others**: Besides the counts of antibody, T-helper cells and cytotoxic T-cells, C-ImmSim tool also predicted the B cell populations, cytokines, etc. Based on the Figs. S11-S15, all four vaccine candidates and GII.4C have comparative capable of inducing B cell population, Macrophage (MA) population, natural killer cell population, Dendritic Cell (DC) population, etc. Two high peaks in total cytokines and interleukins (Fig. S15k) were observed after the twice administration of GII.4C, while only one peak could be observed after the twice administration of Vac-VP1-VP2(Fig. S13k). The peak of IFN-γ induced by Vac-VP1-VP2 and GII.4C could achieve 400,000 ng/ml. While the count of IL-2 induced by Vac-VP1-VP2 was the highest could over 500,000 ng/ml, which were superior to the validated vaccine GII.4C (positive control) with only induced < 450,000 ng/ml (Fig. S13k & Fig. S15k).

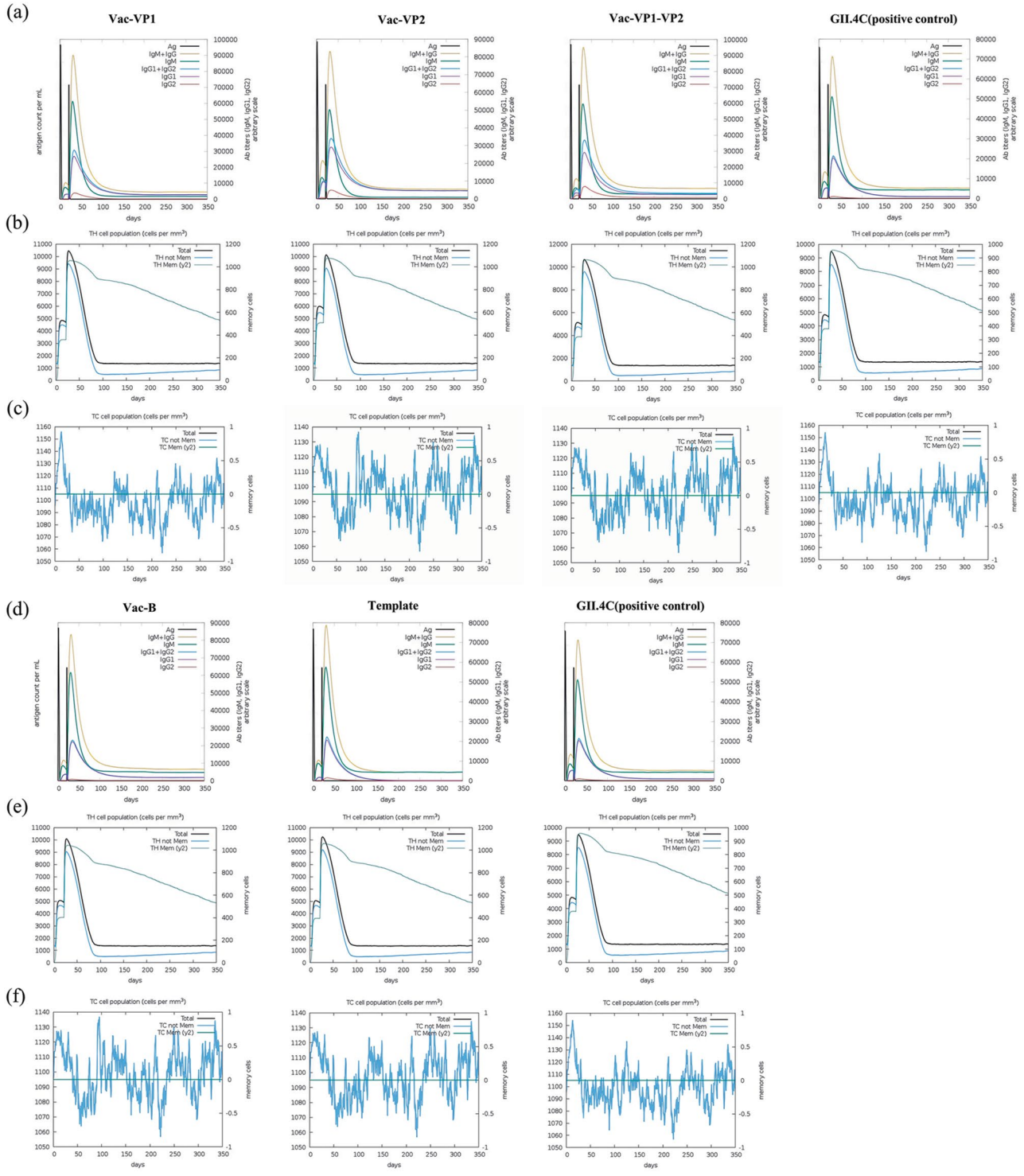

Fig. 5 Simulation of immune response induced by vaccine constructs and GII.4C: (**a**) Antibody response of designed T-cell multi-epitope vaccines and GII.4C. Different colors reflect the diverse subtypes of immunoglobulins; (**b**) The count of T-helper cells after injection of designed T-cell multi-epitope vaccines and GII.4C; (**c**) The count of cytotoxic T lymphocyte population after vaccine injection of designed T-cell multi-epitope vaccines and GII.4C; (**d**) Antibody response of Vac-B, template protein and GII.4C; (**e**) The count of T-helper cells after injection of Vac-B, template protein and GII.4C; (**f**) The count of cytotoxic T lymphocyte population after antigen injection of Vac-B, template protein and GII.4C

In general, the vaccine constructs designed in this study induced the generation of immune molecules and triggered effective immune responses, with Vac-VP1-VP2 showing the strongest response. The immune response was stronger or comparable to the reported norovirus vaccine candidate GII.4C.

The immune simulation result of Vac-B vaccine construct

To test the potential of Vac-B as a subunit vaccine, the immune response was predicted. The reported vaccine GII.4C, along with the template protein AY675554, were also tested for comparison. It was observed that after vaccine immunization, the host immune response was significantly activated (Fig. 5).

1. **Antibody Concentration**: After the first injection of all vaccine antigens, antibody titres began to rise and reached a minor peak within a few days. Vac-B and the template protein triggered lower antibody titres than GII.4C. After the second dose, all the antibody titres peaked, and Vac-B induced the highest titre scale of close to 90,000 per ml. The antibody titre induced by the template protein was close to 80,000 per ml, both much superior to the 70,000 titre per ml induced by GII.4C. Subsequently, all antibody titres began to decline rapidly after 30 days of vaccine injection and became stable at 100 days. The antibody titres of Vac-B and the template protein were comparable to GII.4C after 350 days of injections (Fig. 5d).
2. **Immune Cell Count**: After the first administration, all the antigens induced a small peak in the helper T cell population. The number of total T-helper cells and memory cells reached their highest peaks after the second administration. The peak of total T-helper cells for Vac-B and the template was over 10,000 cells per mm^3, which was higher than GII.4C. The peaks of memory cells for Vac-B and the template were over 1,000 cells per mm^3, which were superior to GII.4C. After the second peak, the number of total T-helper cells began to decline rapidly and eventually stabilised at a low level. After the gradual decline, around 350 days, the number of T-helper memory cells for Vac-B and the template was close to 600 cells per mm^3, slightly greater than GII.4C (Fig. 5e).

For the count of cytotoxic T-cells, the peaks of Vac-B and the template were close to 1,130 cells per mm^3 after the first administration, slightly lower than GII.4C. However, an effective amount of cytotoxic T-cells was still triggered (Fig. 5f).

Two peaks of cytokines and interleukins could be observed after the twice administration of GII.4C and Vac-B, and the large scale of IFN-γ induced by Vac-B was equivalent to GII.4C. The large titer scales of IL-2 induced by Vac-B was over 450,000 ng/ml, which were superior to the validated vaccine GII.4C (positive control) with only induced < 450,000 ng/ml (Figs. S14k-S15k).

In summary, the Vac-B designed in this study successfully induced an immune response that was superior to or equivalent to the reported norovirus vaccine candidate GII.4C.

Molecular dynamic simulations of the docked complexes

The dynamic simulation of four vaccine constructs and positive GII.4C, were conducted and evaluated by iMODS and CABS-flex (Fig. 6). The motion direction on molecular simulation was illustrated on Fig. 6a. In the general evaluation of motion stiffness, the eigenvalue was calculated reflecting the energy required for structure deformation (Fig. 6b). For Vac-VP1, Vac-VP2, Vac-VP1-VP2, Vac-B and GII.4C, the eigenvalues were 4.69×10^{-5}, 2.83×10^{-6}, 2.43×10^{-5}, 4.81×10^{-5} and 5.94×10^{-5}, respectively. Note that, lower value refers to easier deformation. Among these vaccine constructs, Vac-VP2 obtained the lowest value indicating low modal stiffness, the result is consistent with the worst Z-score in homology modelling. Positive control of GII.4C protein obtained the highest value which indicated the high structure stability, this may due to that GII.4C was the consensus sequence of VP1 protein, which was theoretically similar to nature protein. In the detail region of deformation (Fig. 6c), residue region of 320–420 (Vac-VP1), 30–40(Vac-VP2), 80–90(Vac-VP2), 90–100(Vac-VP1-VP2), 620–630(Vac-VP1-VP2), 0–10(Vac-B), 50–60(Vac-B), 0–25(GII.4 C), 410–420(GII.4 C) obtained the high deformability score, which may suggest the hinges or loop region. In structure flexibility evaluation (Fig. 6d), root mean square fluctuation (RMSF) for coordination of each atom in MD were calculated. Taken 3Å as a reference, there were 88.01%, 29.61%, 92.90%, 92.55%, 95.60% residues with RMSF less than 3Å for above proteins. The result indicated structure of Vac-VP2 was flexible, for Vac-VP1 and Vac-B, the majority of more than 90% residues obtained stable in MD, which is comparable to GII.4C. In conclusion, for the four vaccine constructs, in molecular simulation, the multi-epitope Vac-VP1-VP2 and Vac-B could have stable 3D structure, as well as the consensus protein of GII.4C.

Codon optimization and in Silico cloning of the vaccine construct

The codon optimization of vaccine proteins is a significant step for computational design of vaccines, the successful expression of vaccine candidates would be allowed for future production and purification [105]. Since the degeneracy of codons, the sequence of designed vaccines should fit the preference of targeted hosts to improve the

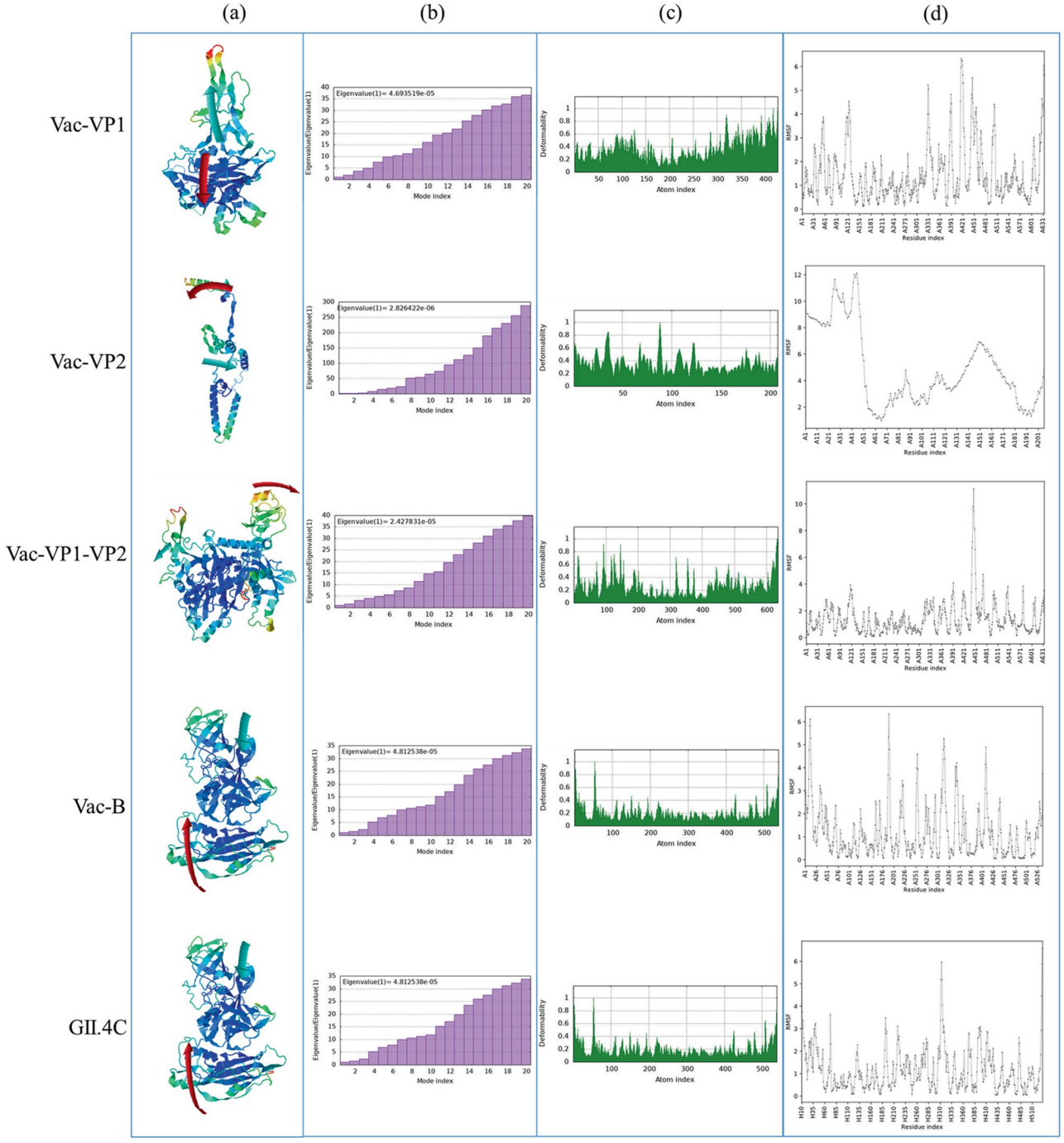

Fig. 6 Molecular dynamic simulation of vaccine constructs. (**a**) protein structure, the affine-model arrows representation of domain dynamics; (**b**) eigenvalue; (**c**) deformability; (**d**) RMSF

expression in the heterologous hosts. The JCat tool was used to codon optimization, and *Escherichia coli* (strain K12), *Saccharomyces cerevisiae*, and *Homo sapiens* were selected as targeted hosts, the predicted CAI index and CG-content were used to assess the express degree of vaccine sequence. The CAI value between 0.8 and 1.0 is favorable, and the larger the better, the score of GC-content between 30 and 70% would be seen as ideal [105].

The predicted values of four vaccine candidates were listed in Table 3, all four vaccines would achieve high expression in *E. coli* K12 and *Saccharomyces cerevisiae*. The GC-Content of Vac-VP1, Vac-VP2, and Vac-VP1-VP2 were little higher than 70% in *Homo sapiens*, which might affect the expression of the vaccines. The adapted sequences of vaccine candidates in E. coli K12 were incorporated into pET30a(+) vector along with XhoI and

Table 3 The values of adapted vaccine candidates

Host strain	value	Vac-VP1	Vac-VP2	Vac-VP1-VP2	Vac-B
Escherichia coli (strain K12)	CAI	1.0	1.0	1.0	1.0
	GC-Content(%)	57.18	55.18	56.52	56.11
Saccharomyces cerevisae	CAI	0.98	0.98	0.98	0.98
	GC-Content(%)	46.67	46.44	46.64	44.26
Homo sapiens	CAI	0.96	0.96	0.96	0.96
	GC-Content(%)	71.84	71.68	71.82	69.09

BamHI restriction sites. The cloning results of other vaccine candidates could be seen in Fig. S16.

In vitro expression and purification of the Vac-B and Vac-VP1-VP2 and In-Vivo evaluation of its immunological properties

The full length of Vac-B and Vac-VP1-VP2 proteins were artificially synthesised and linked to pET-30a. The recombinant plasmids pET-30a-Vac-B and pET-30a-Vac-VP1-VP2 were successfully constructed. SDS-PAGE electrophoresis showed that the molecular weight of the recombinant Vac-B protein is 59.53 kDa, and the molecular weight of the Vac-VP1-VP2 protein is 67.85 kDa (Fig. 7a), which are consistent with the computationally predicted sizes of 58.45 kDa and 66.65 kDa (the uncropped SDS-PAGE gel image of Vac-VP1-VP2 and Vac-B could be seen in Fig. S17).

Western blot analysis confirmed the presence of the target proteins VB and V1/2 in the purified samples. Distinct immunoreactive bands were observed at the expected molecular weights of 58.45 kDa and 66.65 kDa, respectively. These findings indicate successful expression and purification of the vaccine immunogen protein.

Overall, the results demonstrate that the antibody specifically and reliably detects the target proteins under the conditions used, supporting both the identity and integrity of the purified protein (Fig. S18).

Vac-B- and Vac-VP1-VP2-specific IgG levels in the serum measured by ELISA

To determine the humoral immune effects induced by Vac-B and Vac-VP1-VP2 proteins, we assessed serum IgG and IgA levels using enzyme-linked immunosorbent assay (ELISA). The results showed that the IgG titres induced by the two proteins against various norovirus serotypes were above the cut-off value, indicating that each of these proteins was capable of inducing a robust immune response against various serotypes of norovirus. Furthermore, there were differences in the serum-specific IgG responses against different serotypes of norovirus VLP proteins induced by the vaccines (Fig. 7c). The level of GI.1 and GII.3-VLP specific IgG binding antibodies induced by the Vac-VP1-VP2 protein was significantly higher than that induced by Vac-B ($P<0.05$). Conversely, the level of GII.2, GII.4, GII.6, and GII.17-VLP specific IgG binding antibodies induced by Vac-B was significantly higher than that induced by Vac-VP1-VP2 ($P<0.05$). The Vac-VP1-VP2 protein was most effective in inducing GI.1 specific IgG antibodies, with a geometric mean titre (GMT) reaching 9.2×10^3 (95% CI: 6.1×10^3 – 1.3×10^4). The Vac-B protein induced the highest level of GII.4 specific IgG antibodies in the serum, with a GMT of 2.2×10^8 (95% CI: 9.4×10^7– 4.0×10^8).

Vac-B- and Vac-VP1-VP2-specific IgA levels in the serum measured by ELISA

As shown in Fig. 7d, the ability of Vac-B and Vac-VP1-VP2 proteins to induce serum IgA levels was lower than their ability to induce serum IgG levels. The IgA titers induced by the Vac-VP1-VP2 protein against norovirus serotypes were above the cut-off value (except GII.3). The levels of GI.1, GII.3, and GII.4-VLP specific IgA binding antibodies induced by Vac-VP1-VP2 were significantly higher than those induced by Vac-B. Meanwhile, the IgA titre induced by Vac-B protein against GII.2, GII.4, GII.6, and GII.17 were above the cut-off value, and the levels of GII.2 and GII.17-VLP specific IgA binding antibodies induced by Vac-B were significantly higher than those induced by Vac-VP1-VP2. The Vac-VP1-VP2 protein was most effective in inducing GII.4 specific IgA antibodies, with a GMT reaching 2.6×10^4 (95% CI: -2.5×10^4–7.8×10^4), which is close to that induced by the hexavalent vaccine (GMT 4.6×10^4). The IgA levels for GII.2 and GII.17 induced by Vac-B were superior to the other four genotypes, with a GMT value over 2.3×10^5(95% CI: -3.1×10^5– 7.7×10^5), which is close to the GII.17-VLP specific IgA binding antibodies induced by the hexavalent vaccine (GMT 2.6×10^5).

Although the levels of specific IgG and IgA binding antibodies induced by both proteins against most norovirus serotypes were lower than those induced by the hexavalent vaccine, there are still some exciting findings:

1. The level of IgG binding antibodies specific to GII.2-VLP induced by Vac-VP1-VP2 and Vac-B proteins was higher than that induced by the hexavalent vaccine, with the titre induced by Vac-B being the highest. The GII.2 genotype has caused large outbreaks of acute gastroenteritis in many countries

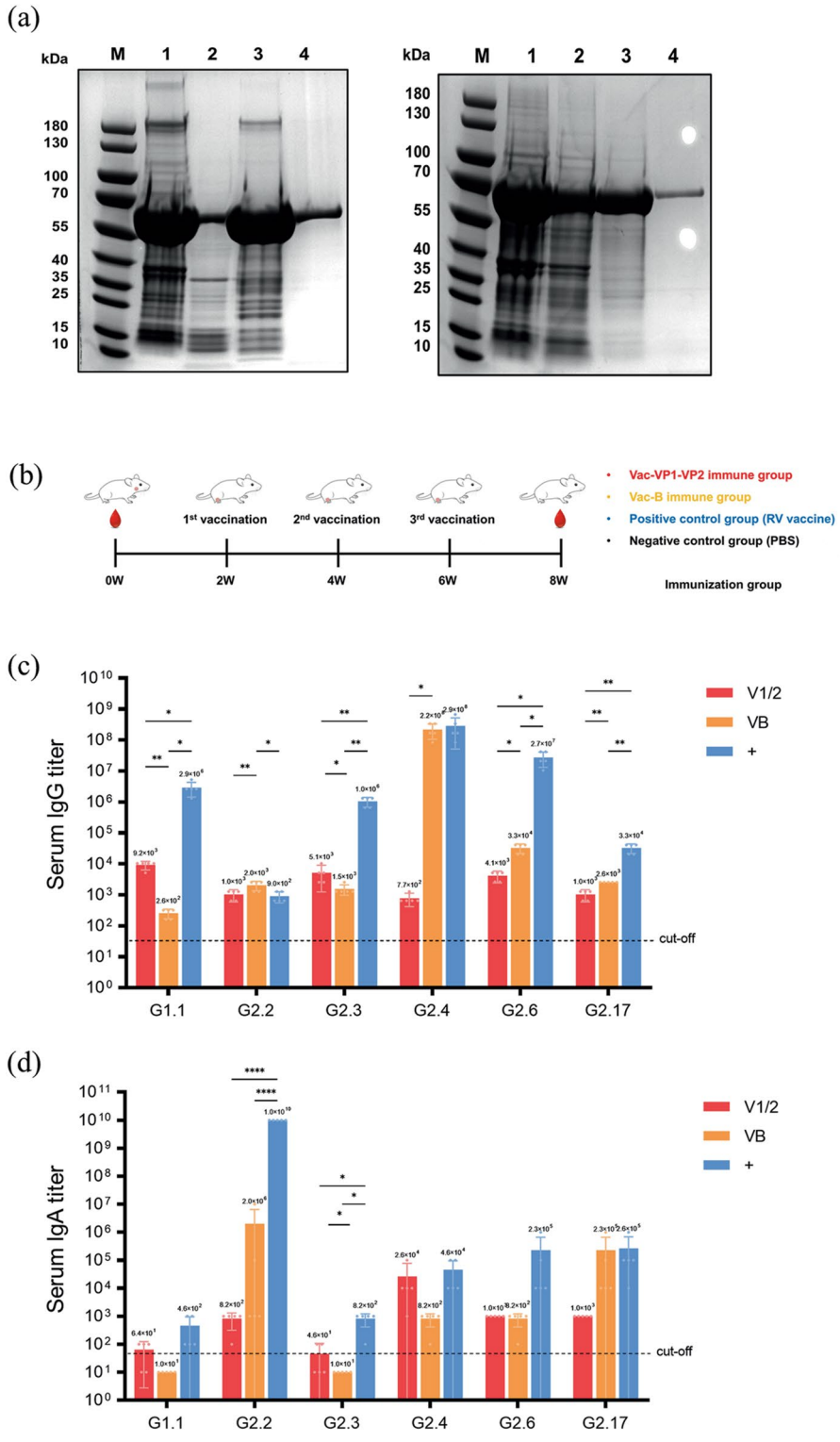

Fig. 7 Immune responses elicited by designed vaccines. (**a**) SDS-PAGE analysis of proteins. On the left is the SDS-PAGE analysis of Vac-B proteins, and on the right is the SDS-PAGE analysis of Vac-VP1-VP2 proteins. 1: Induced Supernatant; 2: Purified Product 1; 3: Induced Supernatant; 4: Purified Concentrated Product 2; M: Protein Molecular Weight Standard; (**b**) Timeline for active immunization with the designed vaccine regimen, comprising three vaccinations with a two-week interval. Mice were stratified into the Vac-VP1-VP2 immunized group, Vac-B immunized group, positive control group, and negative control group; (**c**) Serum NoV genotype-specific IgG antibody titers in Vac-B and Vac-VP1-VP2 immune sera; (**d**) Serum NoV genotype-specific IgA antibody titres in Vac-B and Vac-VP1-VP2 immune sera. Results were displayed as geometric mean titre (GMT) with 95% CI. The dotted line is the cut-off. The logarithm (log10) of the original antibody titres was taken, and statistical differences between groups were assessed using a group t-test. Ns (not statistically significant), $P > 0.05$; *, $P < 0.05$; **, $P < 0.01$; ***, $P < 0.001$; ****, $P < 0.0001$

[106] and, together with GII.4, has been considered one of the most common genotypes [107].
2. There was no significant difference in lgG antibody levels against GII.4 between those induced by Vac-B (GMT 2.2×10^8, 95% CI: $9.4 \times 10^7 - 4.0 \times 10^8$) and those induced by the hexavalent vaccine (GMT 2.9×10^8, 95% CI: $8.3 \times 10^7 - 5.9 \times 10^8$) ($P > 0.05$).
3. There was no significant difference in lgA antibody levels against GII.17 between those induced by Vac-B and those induced by the hexavalent vaccine, nor between Vac-VP1-VP2 and the hexavalent vaccine for GII.4-VLP specific lgA levels.

Based on these findings, Vac-B and Vac-VP1-VP2 developed in this study have demonstrated the ability to elicit an immune response against several norovirus genotypes and show the potential to provide broad cross-protection. Furthermore, the designed vaccines are superior to the existing hexavalent vaccine to a certain extent, indicating a promising potential for future development.

Discussion

Norovirus-induced acute gastroenteritis has become a critical public health issue worldwide, while vaccines can be an effective way of prevention and treatment [108]. To date, there are no licensed vaccines for NoVs, and only a few vaccine candidates have been granted approval for clinical trials, including HIL-216, the first clinically licensed hexavalent VLP vaccine candidate for NoVs [109]. Both VLP and epitope-based vaccines are promising alternatives of traditional platforms, but there are several differences between them. In terms of safety, VLP vaccines utilize self-assembling particles composed of proteins, mimicking the virus structure without containing infectious genetic material, which reduces the risk of adverse effects and provides great safety [110]. On the contrary, epitope-based vaccines only employed the minimal antigenic epitopes of target proteins, which are considered an intrinsically safe approach [111]. On the terms of efficacy, peptides exhibit weak immunogenicity when used alone, which requires the use of other adjuvants or an appropriate delivery system to enhance their efficacy. Meanwhile, VLPs are composed of protein components with highly ordered structures and varying degree of complexity, which could offer higher immunogenicity [112]. Furthermore, compared with VLP vaccines, epitope-based vaccines have higher immune target and specificity [113]. Considering the production process, the antigens of VLP vaccines are much larger than epitopes, which may bring the risk of stability issues, large-scale protein and expression difficulties [113]. In this study, we developed a de novo pipeline, TSBSline (a pipeline designed based on the T-cell site screening strategy and B-cell spatial epitope), which integrates multiple bioinformatics technologies to design the epitope-based vaccine candidates for NoVs. Comprehensive validations of both in silico and in vivo experiments confirmed the rational, broad-spectrum potential, and immunogenicity of the vaccine candidates designed by our pipeline.

The successful design of vaccine candidates relies on our pipeline, which enables the vaccines to have the potential for cross-protection across different strains. Focus on the major circulating norovirus strains may lead to vaccines exhibiting unsatisfactory broad-spectrum performance in less studied but still important strains [8]. In our study, the most comprehensive protein sequence dataset of capsid proteins VP1 and VP2 was constructed based on a database that covers all genotypes that can infect humans. The antigen proteins of the designed vaccines are consensus sequences of all genotypes' VP1 and VP2 proteins. The application of consensus sequences could obtain the conserved parts of all 212 VP1 and 146 VP2 proteins from diverse viral genotypes, providing the potential for cross-protection against different strains. The potential of preventing infections by different strains using consensus sequences has been proven in Lu's study [114]. We also introduced the GII.4 C protein sequence as the positive control to validate the effectiveness of the proposed vaccine candidates, which has been widely used in the development of multivalent VLP-based vaccines [115] and is composed of the consensus sequence of three NoV GII.4 strains.

Besides the abundance of the dataset, we also proposed novel strategies for computationally designing broad-spectrum epitopes. For the construction of T-cell broad-spectrum multi-epitope vaccines, numerous peptides from VP1 and VP2 proteins were generated using the MHC-I and MHC-II binding predictions from IEDB. The peptides that could bind to a large number of HLA alleles with high affinity were considered potential T-cell epitopes. In light of the potential epitope pool, the common screening strategy in current studies is to subject the predicted peptides to a series of filters, and the peptides that meet all specified criteria are identified as epitopes for subsequent vaccine development [116, 117]. However, we defined a new site-based strategy for constructing broad-spectrum epitopes (detailed information can be found in *Methods T cell Multi-Epitope Vaccine Construct*). The epitopes we obtained are more flexible in length, which could provide a high binding affinity with more HLA alleles and achieve higher population coverage. By connecting epitopes derived from VP1 or VP2 proteins with linkers, we constructed three vaccine candidates: Vac-VP1, Vac-VP2, and Vac-VP1-VP2.

For the development of B-cell broad-spectrum multi-epitope vaccines, we first constructed a dataset of known B-cell spatial epitope positions based on published papers. Then, the residue positions of known epitopes

were mapped to the 3D structures of VP1 proteins constructed earlier. The broad-spectrum epitopes were screened by high-throughput calculation of the antigenicity similarity between epitopes using the computational method CE-BLAST. Finally, the broad-spectrum epitopes were assembled to obtain the B-cell multi-epitope vaccine Vac-B. Vac-B covers 10 broad-spectrum epitopes, providing over 53.16–98.95% antigenic coverage of all VP1 proteins, with the joint coverage reaching 100% and the average coverage reaching 71.58%. The 10 epitopes were also mapped to the GII.4C model. The performance of Vac-B was better than the GII.4C model in both individual and joint coverage of the 10 epitopes, indicating that Vac-B performs excellently in broad-spectrum coverage and is superior to the reported norovirus vaccine candidate GII.4C. The constructed pipeline endows the vaccine with the ability to cross-protect against different virus strains and makes great use of the immune potential of B-cell spatial epitopes, providing a new perspective for the future application of spatial conformation epitopes.

Computational analyses revealed promising physicochemical properties, immunogenicity, rational structures, stability, and binding potential with TLR7 for all designed vaccines. While the structural rationality of designed vaccine candidates have been verified by several tools, disulfide engineering still is a great way to increase the stability of the vaccine construct, thus the Disulfide by Design 2.0 [118] with the default parameters, was introduced to design disulfide bonds in the vaccine structures. Considering that 90% of native disulfides have an energy value less than 2.2 kcal/mol [118], there were only 8 for Vac-VP1 (135LEU-139TRP, 386THR-397GLY, 176LEU-185SER, 18ALA-315PRO, 174ALA-198PHE, 342GLU-391GLY, 42ALA-58ILE, 11PRO-257GLY), 1 for Vac-VP2 (111GLY-128GLY), 10 for Vac-VP1-VP2 (337GLY-485PRO, 425PHE-578GLY, 490LEU-510VAL, 511PRO-514GLY, 318VAL-481ALA, 21SER-96THR, 252THR-254GLN, 344LYS-84THR, 297PRO-420SER, 283ALA-309THR), 2 for Vac-B (36ALA-164TYR, 120ALA-141HIS) fit the energy requirement and compatible for disulfide bond formation. The targeted residues were replaced by cysteine amino acid as represented by red sticks in the mutated structure in Fig. S19.

Regarding the immunity of the developed vaccines, we have detected it by computational tools and in vivo mouse immune experiments. The in silico simulation results demonstrate that the designed vaccines have the ability to elicit a robust immune response, with their performance surpassing that of the positive control group. Vac-VP1-VP2 and Vac-B exhibited the best results. In vitro experiments, SDS-PAGE electrophoresis showed that the designed vaccines could be successfully expressed and purified, and the actual molecular weight value (59.53 kDa for Vac-B and 67.85 kDa for Vac-VP1-VP2) is in accordance with the prediction from the bioinformatics tool (58.45 kDa for Vac-B and 66.65 kDa for Vac-VP1-VP2). ELISA results demonstrated a substantial increase in serum levels of various NoV genotype-specific IgG and IgA antibodies induced by Vac-VP1-VP2 and Vac-B immunization. Furthermore, Vac-VP1-VP2 and Vac-B can evoke robust immune responses against 6 common norovirus genotypes (over the cut-off, with the highest titer reaching GMT 2.2×10^8, 95% CI: 9.4×10^7–4.0×10^8). The ability to induce high IgG antibody titres was also consistent with the results of computational simulations. The experimental results exhibited the immunogenicity and broad-spectrum nature of the designed vaccines, which were superior to the baseline and equally comparable to the multi-type VLPs, similar to candidate vaccines currently in development.

Conclusion

Our research presents an innovative and reliable pipeline for developing multi-epitope vaccines with broad-spectrum coverage, which makes great use of the immune potential of B-cell conformational epitopes and T-cell linear epitopes. Meanwhile, we have also identified the limitations of our work that may be addressed in future studies. For example, real population coverage in local areas may require cohort studies for determination, the binding affinity of broad-spectrum epitope-HLA complexes requires experimental validation, and the selection of suitable linkers and adjuvants needs further optimization. In summary, the pipeline designed in this study provides potential tools for vaccine design. Moreover, the Vac-B and Vac-VP1-VP2 vaccines designed using this pipeline are promising candidates against norovirus, which may provide novel approaches for the active prevention and control of norovirus worldwide.

Supplementary Information

The online version contains supplementary material available at https://doi.org/10.1186/s12985-025-02796-6.

Supplementary Material 1
Supplementary Material 2
Supplementary Material 3
Supplementary Material 4
Supplementary Material 5
Supplementary Material 6
Supplementary Material 7
Supplementary Material 8
Supplementary Material 9
Supplementary Material 10
Supplementary Material 11

Supplementary Material 12
Supplementary Material 13
Supplementary Material 14
Supplementary Material 15
Supplementary Material 16
Supplementary Material 17
Supplementary Material 18
Supplementary Material 19
Supplementary Material 20
Supplementary Material 21
Supplementary Material 22
Supplementary Material 23
Supplementary Material 24
Supplementary Material 25
Supplementary Material 26
Supplementary Material 27
Supplementary Material 28
Supplementary File 2
Supplementary File 3

Acknowledgements
This work is supported by the Medical Science Data Center of Fudan University. This work was supported by grants from the National Key Research and Development Program of China (2022YFF1101104, 2022YFF1103101), the National Natural Science Foundation of China (32370697).

Author contributions
JXQ and YWW performed all bioinformatics assays, analyses, and writing the manuscript. JYS and WJZ performed all experimental assays and analyses. YXZ, JTX, DZ, and XCL contributed to analyzing bioinformatics assays and collected the literature. XLS, WJZ and XW modified the manuscript. SJW, XYW, and TYQ supervised the whole project.

Funding
This work was supported by grants from the National Key Research and Development Program of China (2022YFF1101104, 2022YFF1103101), the National Natural Science Foundation of China (32370697).

Data availability
No datasets were generated or analysed during the current study.

Declarations

Ethics approval and consent to participate
All animal experiments were conducted following the standards set by the Ethics Committee of Fudan University.

Consent for publication
Not applicable.

Competing interests
The corresponding author Tianyi Qiu is an editor board member of Virology Journal.

Author details
[1]School of Health Science and Engineering, University of Shanghai for Science and Technology, Shanghai 200093, China
[2]Institute of Clinical Science, Clinical Center of Biotherapy, Zhongshan Hospital, Shanghai Institute of Infectious Disease and Biosecurity, Intelligent Medicine Institute, Shanghai Medical College, Fudan University, 200032 Shanghai, China
[3]Institutes of Biomedical Sciences; Shanghai Institute of Infectious Disease and Biosecurity, Key Laboratory of Medical. Molecular Virology of MoE&MoH, Shanghai Medical College, Fudan University, 200032 Shanghai, China
[4]State Key Laboratory of Food Science and Technology, School of Food Science and Technology, National Engineering Research Center for Functional Foods, Synergetic Innovation Center of Food Safety and Nutrition, Jiangnan University, Wuxi, Jiangsu, 214122, China
[5]Shanghai Collaborative Innovation Center of Energy Therapy for Tumors, Shanghai 200093, China

Received: 9 February 2025 / Accepted: 15 May 2025
Published online: 27 May 2025

References

1. Hong X, Xue L, Gao J, Jiang Y, Kou X. Epochal coevolution of minor capsid protein in norovirus GII.4 variants with major capsid protein based on their interactions over the last five decades. Virus Research. 319:198860, 2022/10/02/ 2022.
2. de Graaf M, van Beek J, Koopmans MPG. Human Norovirus transmission and evolution in a changing world. Nat Rev Microbiol. 14(7):421–33, 2016/07/01 2016.
3. Robilotti E, Deresinski S, Pinsky Benjamin A. Norovirus. Clin Microbiol Rev. 2015;28(1):134–64.
4. Soorneedi AR, Moore MD. Recent developments in Norovirus interactions with bacteria. Curr Opin Food Sci. 2022:48.
5. Hardy ME. Norovirus protein structure and function. FEMS Microbiol Lett. 2005;253(1):1–8.
6. Chhabra P, et al. Updated classification of Norovirus genogroups and genotypes. J Gen Virol. 2019;100(10):1393–406.
7. Kobayashi M et al. Molecular evolution of the capsid gene in human Norovirus genogroup II. Sci Rep. Jul 7 2016;6:29400.
8. Azim KF et al. Immunoinformatics approaches for designing a novel multi epitope peptide vaccine against human Norovirus (Norwalk virus). Infect Genet Evol. 2019:74.
9. Esposito S, Principi N. Norovirus vaccine: priorities for future research and development. Front Immunol. 2020:11.
10. Cates JE, Vinjé J, Parashar UD, Hall AJ. Recent advances in human Norovirus research and implications for candidate vaccines. Expert Rev Vaccines. 2020;19:539–48.
11. Cortes-Penfield NW, Ramani S, Estes MK, Atmar RL. Prospects and challenges in the development of a Norovirus vaccine. Clin Ther. 2017;39(8):1537–49. 2017/08/01/.
12. Rappuoli R, Bottomley MJ, D'Oro U, Finco O, De Gregorio E. Reverse vaccinology 2.0: human immunology instructs vaccine antigen design. J Exp Med. 2016;213:469–81.
13. Hameed AR et al. Exploring the hub genes and potential drugs involved in Fanconi anemia using microarray datasets and bioinformatics analysis. J Biomol Struct Dynamics. 2025;43(7):3297–310, 2025/05/03 2025.
14. Ahmad S et al. Identification of potential drug molecules against fibroblast growth factor receptor 3 (FGFR3) by multi-stage computational-biophysics correlate. J Biomol Struct Dynamics. 2025;43(3):1240–8, 2025/02/11 2025.
15. Khan N et al. A novel therapeutic approach to prevent Helicobacter pylori induced gastric cancer using networking biology, molecular docking, and simulation approaches. J Biomol Struct Dynamics. 2024;42(24):13876–89, 2024/12/20 2024.
16. Aftab N, et al. An optimized deep learning approach for blood-brain barrier permeability prediction with ODE integration. Inf Med Unlocked. 2024;48:101526. 2024/01/01/.
17. Zhang L. Multi-epitope vaccines: a promising strategy against tumors and viral infections. Cell Mol Immunol. 2018;15(2):182–4, 2018/02/01 2018.
18. Yuan L et al. In silico design of a broad-spectrum multiepitope vaccine against influenza virus, *International Journal of Biological Macromolecules*, vol. 254, p. 128071, 2024/01/01/ 2024.
19. Ullah A et al. Bioinformatics and immunoinformatics approach to develop potent multi-peptide vaccine for coxsackievirus B3 capable of eliciting

cellular and humoral immune response, *International Journal of Biological Macromolecules*, vol. 239, p. 124320, 2023/06/01/ 2023.
20. Tahir Ul Qamar M et al. Development of a novel Multi-Epitope vaccine against Crimean-Congo hemorrhagic fever virus: an integrated reverse vaccinology, vaccine informatics and biophysics approach, (in English). Frontiers Immunol Original Res 12, 2021-June-16 2021.
21. Farzan M et al. Immunoinformatics-based multi-epitope vaccine design for the re-emerging monkeypox virus, *International Immunopharmacology*, vol. 123, p. 110725, 2023/10/01/ 2023.
22. Pourseif MM et al. A domain-based vaccine construct against SARS-CoV-2, the causative agent of COVID-19 pandemic: development of self-amplifying mRNA and peptide vaccines, *BioImpacts*, vol. 11, no. 1, pp. 65–84, 2021/1/1 2021.
23. Pourseif MM et al. A novel in silico minigene vaccine based on CD4 + T-helper and B-cell epitopes of EG95 isolates for vaccination against cystic echinococcosis, *Computational Biology and Chemistry*, vol. 72, pp. 150–163, 2018/02/01/ 2018.
24. Majidiani H, Pourseif MM, Kordi B, Sadeghi M-R, Najafi A. TgVax452, an epitope-based candidate vaccine targeting Toxoplasma gondii tachyzoite-specific SAG1-related sequence (SRS) proteins: immunoinformatics, structural simulations and experimental evidence-based approaches. BMC Infect Dis, 24, 1, p. 886, 2024/08/29 2024.
25. Parvizpour S, Pourseif MM, Razmara J, Rafi MA, Omidi Y. Epitope-based vaccine design: a comprehensive overview of bioinformatics approaches. Drug Discovery Today. 2020;25(6):1034–42. 2020/06/01/.
26. Høie MH et al. DiscoTope-3.0: improved B-cell epitope prediction using inverse folding latent representations, (in English), *Frontiers in Immunology*, Technology and Code vol. 15, 2024-February-08 2024.
27. Sun J, et al. SEPPA: a computational server for Spatial epitope prediction of protein antigens. Nucleic Acids Res. 2009;37:W612–6.
28. Krawczyk K, Liu X, Baker TS, Shi J, Deane CM. Improving B-cell epitope prediction and its application to global antibody-antigen Docking. Bioinformatics. 2014;30:2288–94.
29. Oyarzún P, Ellis JJ, Bodén M, Kobe B. PREDIVAC: CD4 + T-cell epitope prediction for vaccine design that covers 95% of HLA class II DR protein diversity. BMC Bioinformatics, 14, 1, p. 52, 2013/02/14 2013.
30. Singh H, Raghava GPS. ProPred1: prediction of promiscuous MHC Class-I binding sites, *Bioinformatics*, vol. 19, no. 8, pp. 1009–1014, 2003.
31. Buus S, et al. Sensitive quantitative predictions of peptide-MHC binding by a 'query by committee' artificial neural network approach. Tissue Antigens. 2003;62(5):378–84.
32. Dimitrov I, Garnev P, Flower DR, Doytchinova I. EpiTOP—a proteochemometric tool for MHC class II binding prediction, *Bioinformatics*, vol. 26, no. 16, pp. 2066–2068, 2010.
33. Kumar N, Bajiya N, Patiyal S, Raghava GPS. Multi-perspectives and challenges in identifying B-cell epitopes. Protein Sci, 32, 11, p. e4785, 2023/11/01 2023.
34. Ahmad I et al. Development of multi-epitope subunit vaccine for protection against the Norovirus' infections based on computational vaccinology. J Biomol Struct Dynamics, 40, 7, pp. 3098–109, 2022/05/03 2022.
35. Shanthappa PM, Suravajhala R, Suravajhala P, Kumar G, Melethadathil N. In Silico based multi-epitope vaccine design against Norovirus. J Biomol Struct Dynamics, 41, 12, pp. 5696–706, 2023/08/13 2023.
36. Larkin MA et al. Clustal W and Clustal X version 2.0, *Bioinformatics*, vol. 23, no. 21, pp. 2947–2948, 2007.
37. Madeira F et al. The EMBL-EBI job dispatcher sequence analysis tools framework in 2024, (in eng). Nucleic Acids Res, 52, no. W1, pp. W521-W525, 2024/07// 2024.
38. Eswar N et al. Comparative protein structure modeling using modeller. Curr Protocols Bioinf 15, 2006.
39. Baek M et al. Accurate prediction of protein structures and interactions using a three-track neural network, *Science*, vol. 373, no. 6557, pp. 871–876, 2021/08/20 2021.
40. Parra GI et al. Immunogenicity and specificity of norovirus Consensus GII.4 virus-like particles in monovalent and bivalent vaccine formulations, *Vaccine*, vol. 30, no. 24, pp. 3580–3586, 2012/05/21/ 2012.
41. van Loben Sels JM, Green KY. The Antigenic Topology of Norovirus as Defined by B and T Cell Epitope Mapping: Implications for Universal Vaccines and Therapeutics, *Viruses*, vol. 11, 2019.
42. Lochridge VP, Jutila KL, Graff JW, Hardy ME. Epitopes in the P2 domain of Norovirus VP1 recognized by monoclonal antibodies that block cell interactions. J Gen Virol. 2005;86(10):2799–806.
43. Kher G et al. Direct Blockade of the Norovirus Histo-Blood group antigen binding pocket by nanobodies. J Virol, 97, 2023.
44. Alvarado G et al. Broadly cross-reactive human antibodies that inhibit genogroup I and II Noroviruses. Nat Commun, 12, 1, p. 4320, 2021/07/14 2021.
45. Yi Y et al. Identification of a Blockade epitope of human Norovirus GII.17. Emerg Microbes Infections, 10, 1, pp. 954–63, 2021/01/01 2021.
46. Yi Y et al. Identification of Human Norovirus GII.3 Blockade Antibody Epitopes, *Viruses*, vol. 13, no. 10. https://doi.org/10.3390/v13102058
47. Weiskopf D et al. Comprehensive analysis of dengue virus-specific responses supports an HLA-linked protective role for CD8 + T cells, *Proceedings of the National Academy of Sciences*, vol. 110, no. 22, pp. E2046-E2053, 2013/05/28 2013.
48. Reynisson B, Alvarez B, Paul S, Peters B, Nielsen M. NetMHCpan-4.1 and NetMHCIIpan-4.0: improved predictions of MHC antigen presentation by concurrent motif Deconvolution and integration of MS MHC eluted ligand data. Nucleic Acids Res, 48, no. W1, pp. W449-W454, 2020.
49. Greenbaum J et al. Functional classification of class II human leukocyte antigen (HLA) molecules reveals seven different supertypes and a surprising degree of repertoire sharing across supertypes, (in eng), *Immunogenetics*, 63, 6, pp. 325–35, 2011/06// 2011.
50. Wang P et al. Peptide binding predictions for HLA DR, DP and DQ molecules, *BMC Bioinformatics*, vol. 11, no. 1, p. 568, 2010/11/22 2010.
51. Qiu T et al. CE-BLAST makes it possible to compute antigenic similarity for newly emerging pathogens. Nat Commun, 9, 1, p. 1772, 2018/05/02 2018.
52. Saha S, Raghava GPS. AlgPred: prediction of allergenic proteins and mapping of IgE epitopes. Nucleic Acids Res, 34, no. suppl_2, pp. W202-W209, 2006.
53. Dimitrov I, Naneva L, Doytchinova I, Bangov I. AllergenFP: allergenicity prediction by descriptor fingerprints, (in eng), *Bioinformatics (Oxford, England)*, vol. 30, no. 6, pp. 846–851, 2014/03// 2014.
54. Doytchinova IA, Flower DR. VaxiJen: a server for prediction of protective antigens, tumour antigens and subunit vaccines. BMC Bioinformatics, 8, 1, p. 4, 2007/01/05 2007.
55. Sharma N, Naorem LD, Jain S, Raghava GPS. ToxinPred2: an improved method for predicting toxicity of proteins. Brief Bioinform. 2022;23(5):bbac174.
56. Magnan CN, Randall A, Baldi P. SOLpro: accurate sequence-based prediction of protein solubility, *Bioinformatics*, vol. 25, no. 17, pp. 2200–2207, 2009.
57. Gasteiger E, et al. Protein identification and analysis tools on the expasy server. In: Walker JM, editor. The proteomics protocols handbook. Totowa, NJ: Humana; 2005. pp. 571–607.
58. Hallgren J et al. DeepTMHMM predicts alpha and beta transmembrane proteins using deep neural networks, *bioRxiv*, p. 2022.04.08.487609, 2022.
59. Buchan DWA, Jones DT. The PSIPRED protein analysis workbench: 20 years on. Nucleic Acids Res, 47, pp. W402 - W407, 2019.
60. Ko J, Park H, Heo L, Seok C. GalaxyWEB server for protein structure prediction and refinement. Nucleic Acids Res, 40, no. W1, pp. W294-W297, 2012.
61. Laskowski RA, MacArthur MW, Moss DS, Thornton JM. PROCHECK: a program to check the stereochemical quality of protein structures. J Appl Crystallogr, 26, 2, pp. 283–91, 1993/04/01 1993.
62. Colovos C, Yeates TO. Verification of protein structures: patterns of nonbonded atomic interactions. Protein Sci, 2, 9, pp. 1511–9, 1993/09/01 1993.
63. Sippl MJ. Recognition of errors in three-dimensional structures of proteins. Proteins Struct Funct Bioinform, 17, 4, pp. 355–62, 1993/12/01 1993.
64. Berman HM, et al. The protein data bank. Nucleic Acids Res. 2000;28(1):235–42.
65. Jones G, et al. Elucidation of protein function using computational Docking and hotspot analysis by cluspro and ftmap. Acta Crystallogr Sect D. 2022;78:690–7. Structural Biology.
66. Laskowski RA. PDBsum: summaries and analyses of PDB structures. Nucleic Acids Res. 2001;29(1):221–2.
67. Abramson J et al. Accurate structure prediction of biomolecular interactions with AlphaFold 3, *Nature*, vol. 630, no. 8016, pp. 493–500, 2024/06/01 2024.
68. Moutaftsi M et al. A consensus epitope prediction approach identifies the breadth of murine TCD8+-cell responses to vaccinia virus. Nat Biotechnol, 24, 7, pp. 817–9, 2006/07/01 2006.
69. Kotturi Maya F, et al. The CD8 + T-Cell response to lymphocytic choriomeningitis virus involves the L antigen: Uncovering new tricks for an old virus. J Virol. 2007;81(10):4928–40.
70. Paul S, et al. HLA class I alleles are associated with Peptide-Binding repertoires of different size, affinity, and immunogenicity. J Immunol. 2013;191(12):5831–9.

71. Rapin N, Lund O, Bernaschi M, Castiglione F. Computational immunology Meets bioinformatics: the use of prediction tools for molecular binding in the simulation of the immune system. PLoS ONE. 2010;5(4):e9862.
72. Kovacs JA, Chacón P, Abagyan R. Predictions of protein flexibility: First-order measures. Proteins Struct Funct Bioinform, 56, 4, pp. 661–8, 2004/09/01 2004.
73. López-Blanco JR, Aliaga JI, Quintana-Ortí ES, Chacón P. iMODS: internal coordinates normal mode analysis server. Nucleic Acids Res, 42, no. W1, pp. W271-W276, 2014.
74. Lopéz-Blanco JR, Garzón JI, Chacón P. iMod: multipurpose normal mode analysis in internal coordinates, *Bioinformatics*, vol. 27, no. 20, pp. 2843–2850, 2011.
75. Jamroz M, Kolinski A, Kmiecik S. CABS-flex: server for fast simulation of protein structure fluctuations. Nucleic Acids Res, 41, no. W1, pp. W427-W431, 2013.
76. Goodswen SJ, Kennedy PJ, Ellis JT. A guide to current methodology and usage of reverse vaccinology towards in Silico vaccine discovery. FEMS Microbiol Rev. 2023;47(2):fuad004.
77. Khan S et al. Identification of a Potential Vaccine against Treponema pallidum Using Subtractive Proteomics and Reverse-Vaccinology Approaches, *Vaccines*, vol. 11, no. 1. https://doi.org/10.3390/vaccines11010072
78. Andongma BT, et al. In Silico design of a promiscuous chimeric multi-epitope vaccine against Mycobacterium tuberculosis. Comput Struct Biotechnol J. 2023;21:991–1004. 2023/01/01/.
79. Greenberg DP et al. Safety and immunogenicity of a quadrivalent inactivated influenza vaccine compared to licensed trivalent inactivated influenza vaccines in adults, *Vaccine*, vol. 31, no. 5, pp. 770–776, 2013/01/21/ 2013.
80. Ayyagari VS, C VT, K AP, Srirama K. Design of a multi-epitope-based vaccine targeting M-protein of SARS-CoV2: an immunoinformatics approach. J Biomol Struct Dynamics, 40, 7, pp. 2963–77, 2022/05/03 2022.
81. Kolla HB, Tirumalasetty C, Sreerama K, Ayyagari VS. An immunoinformatics approach for the design of a multi-epitope vaccine targeting super antigen TSST-1 of Staphylococcus aureus. J Genetic Eng Biotechnol, 19, 1, p. 69, 2021/05/11 2021.
82. Parra GI, et al. Identification of a broadly Cross-Reactive epitope in the inner shell of the Norovirus capsid. PLoS ONE. 2013;8(6):e67592.
83. Eden J-S, Lim KL, White PA. Complete genome of the human Norovirus GIV.1 strain lake Macquarie virus, (in eng). J Virol, 86, 18, pp. 10251–2, 2012/09// 2012.
84. Schrodinger LLC. The AxPyMOL Molecular Graphics Plugin for Microsoft PowerPoint, Version 1.8, November, 2015.
85. Shahrear S, Islam ABMMK. Immunoinformatics guided modeling of CCHF_GN728, an mRNA-based universal vaccine against Crimean-Congo hemorrhagic fever virus, *Computers in Biology and Medicine*, vol. 140, p. 105098, 2022/01/01/ 2022.
86. Huang S et al. Designing a multi-epitope vaccine against coxsackievirus B based on immunoinformatics approaches, (in English). Frontiers Immunol Original Res 13, 2022-November-09 2022.
87. Yu M et al. Design of a Recombinant multivalent epitope vaccine based on SARS-CoV-2 and its variants in immunoinformatics approaches, (in English). Frontiers Immunol Original Res 13, 2022-May-06 2022.
88. Kar T et al. A candidate multi-epitope vaccine against SARS-CoV-2. Sci Rep, 10, 1, p. 10895, 2020/07/02 2020.
89. Wiederstein M, Sippl MJ. ProSA-web: interactive web service for the recognition of errors in three-dimensional structures of proteins, *Nucleic Acids Research*, vol. 35, no. suppl_2, pp. W407-W410, 2007.
90. Messaoudi A, Belguith H, Ben Hamida J. Homology modeling and virtual screening approaches to identify potent inhibitors of VEB-1 β-lactamase. Theor Biol Med Model. 2013;10:22–22.
91. Thukral A et al. A single dose polyanhydride-based nanovaccine against paratuberculosis infection. Npj Vaccines, 5, 1, p. 15, 2020/02/14 2020.
92. Khan T et al. Subtractive proteomics assisted therapeutic targets mining and designing ensemble vaccine against Candida auris for immune response induction, *Computers in Biology and Medicine*, vol. 145, p. 105462, 2022/06/01/ 2022.
93. Nawaz M et al. Genome-Based Multi-Antigenic Epitopes Vaccine Construct Designing against Staphylococcus hominis Using Reverse Vaccinology and Biophysical Approaches, *Vaccines*, vol. 10, no. 10. https://doi.org/10.3390/vaccines10101729
94. Doytchinova IA, Flower DR. Bioinformatic approach for identifying parasite and fungal candidate subunit vaccines. Open Vaccine J. 2008;1:22–6.
95. Vita R et al. The immune epitope database (IEDB): 2024 update. Nucleic Acids Res, 53, no. D1, pp. D436-D443, 2025.
96. Dhanda SK, Vir P, Raghava GPS. Designing of interferon-gamma inducing MHC class-II binders. Biol Direct, 8, 1, p. 30, 2013/12/05 2013.
97. Hassan A et al. Pangenome and immuno-proteomics analysis of Acinetobacter baumannii strains revealed the core peptide vaccine targets. BMC Genomics, 17, 1, p. 732, 2016/09/15 2016.
98. Ikai A. Thermostability and aliphatic index of globular proteins. J Biochem. 1980;88(6):1895–8.
99. Kyte J, Doolittle RF. A simple method for displaying the hydropathic character of a protein. J Mol Biol. 1982;157(1):105–32. 1982/05/05/.
100. Ali M et al. Exploring dengue genome to construct a multi-epitope based subunit vaccine by utilizing immunoinformatics approach to battle against dengue infection. Sci Rep, 7, 1, p. 9232, 2017/08/23 2017.
101. Singh A, Thakur M, Sharma LK, Chandra K. Designing a multi-epitope peptide based vaccine against SARS-CoV-2. Sci Rep, 10, 1, p. 16219, 2020/10/01 2020.
102. Choe J-y, Kelker MS, Wilson IA. Crystal structure of human Toll-Like receptor 3 (TLR3) ectodomain. Science. 2005;309:581–5.
103. Ishii KJ, Koyama S, Nakagawa A, Coban C, Akira S. Host innate immune receptors and beyond: making sense of microbial infections. Cell Host Microbe. 2008;3(6):352–63.
104. Thompson JM, Iwasaki A. Toll-like receptors regulation of viral infection and disease, *Advanced drug delivery reviews*, vol. 60 7, pp. 786– 94, 2008.
105. Wei Y, et al. Advances of computational methods enhance the development of multi-epitope vaccines. Brief Bioinform. 2025;26(1):bbaf055.
106. Li X, Liu H, Rife Magalis B, Kosakovsky Pond SL, Volz EM. Molecular evolution of human Norovirus GII.2 clusters, (in English). Frontiers Microbiol Original Res 12, 2021-March-22 2021.
107. Carlson KB et al. A narrative review of Norovirus epidemiology, biology, and challenges to vaccine development. Npj Vaccines, 9, 1, p. 94, 2024/05/29 2024.
108. Bartsch SM, Lopman BA, Ozawa S, Hall AJ, Lee BY. Global Economic Burd Norovirus Gastroenteritis PLoS One. 2016;11(4):e0151219.
109. HilleVax I. HilleVax and Kangh announce exclusive license agreement for hexavalent VLP Norovirus vaccine candidate outside of China, ed, 2024.
110. Chai S, Wang L, Du H, Jiang H. Achievement and Challenges in Orthohantavirus Vaccines, *Vaccines*, vol. 13, no. 2. https://doi.org/10.3390/vaccines13020198
111. Bárcena J, Zamora-Ceballos M, Blanco E. Design of novel vaccines based on Virus-Like particles. In: Mateu MG, editor. Structure and physics of viruses: an integrated guide. Cham: Springer Nature Switzerland; 2024. pp. 785–821.
112. Saba I, Wani K, Rehman S, Singh V. Platform technologies based on Virus-Like particles (VLPs) for infectious diseases. In: Hameed S, Rehman S, editors. Nanotechnology for infectious diseases. Singapore: Springer Singapore; 2022. pp. 541–53.
113. Skwarczynski M, Toth I. Peptide-based synthetic vaccines. Chem Sci, 7, 2, pp. 842–54, 2016/01/26/ 2016.
114. Lu M et al. Vaccines based on the fusion protein consensus sequence protect Syrian hamsters from Nipah virus infection, *JCI Insight*, vol. 8, no. 23, 12/08/ 2023.
115. Lindesmith LC, et al. Broad Blockade antibody responses in human volunteers after immunization with a multivalent Norovirus VLP candidate vaccine: immunological analyses from a phase I clinical trial. PLoS Med. 2015;12(3):e1001807.
116. Waqas M, et al. Employing an immunoinformatics approach revealed potent multi-epitope based subunit vaccine for lymphocytic choriomeningitis virus. J Infect Public Health. 2023;16(2):214–32. 2023/02/01/.
117. de Oliveira Matos A et al. Immunoinformatics-guided design of a multi-valent vaccine against Rotavirus and Norovirus (ChRNV22), *Computers in Biology and Medicine*, vol. 159, p. 106941, 2023/06/01/ 2023.
118. Craig DB, Dombkowski AA. Disulfide by design 2.0: a web-based tool for disulfide engineering in proteins. BMC Bioinformatics, 14, 1, p. 346, 2013/12/01 2013.

Publisher's note